



Toward understanding the unusual reactivity of mesoporous niobium silicates in epoxidation of C=C bonds with hydrogen peroxide



Irina D. Ivanchikova^a, Igor Y. Skobelev^{a,b}, Nataliya V. Maksimchuk^{a,b}, Eugenio A. Paukshtis^{a,b}, Mikhail V. Shashkov^{a,b}, Oxana A. Kholdeeva^{a,b,*}

^a Borekov Institute of Catalysis, Lavrentieva Avenue 5, Novosibirsk 630090, Russia

^b Novosibirsk State University, Pirogova Street 2, Novosibirsk 630090, Russia

ARTICLE INFO

Article history:

Received 29 June 2017

Revised 15 September 2017

Accepted 15 September 2017

Keywords:

Epoxidation

Heterogeneous catalysis

Hydrogen peroxide

Mesoporous niobium silicate

Kinetics

Mechanism

ABSTRACT

Niobium-containing mesoporous silicates reveal superior activity and selectivity in epoxidation of alkenes using hydrogen peroxide as a green oxidant and, in contrast to mesoporous titanium silicates, catalyze epoxidation of both electron-rich and electron-deficient C=C bonds. This report describes a kinetic and mechanistic investigation of epoxidation of two representative substrates, cyclooctene (CyO) and 2-methyl-1,4-naphthoquinone (MNQ), over two mesoporous niobium silicates with predominantly di(oligo)meric or isolated Nb(V) sites. The observed kinetic regularities did not depend on the state of Nb but were strictly determined by the nature of the organic substrate. The rate law established for CyO is consistent with a mechanism that involves interaction of H₂O₂ with Nb(V) sites to give a hydroperoxy species NbOOH and water, followed by oxygen transfer to a nucleophilic C=C bond, producing an epoxide and regenerating the initial state of the catalyst. This mechanism is strongly supported by stereospecificity in epoxidation of *cis*-alkenes and high heterolytic pathway selectivity in the oxidation of cyclohexene. The NbOOH species is manifested by an absorption feature at 307 nm in diffuse reflectance UV–vis spectra. The addition of a base (NaOAc) causes a shift of the absorption band to 293 nm and produces a rate-retarding effect on the epoxidation reaction. Several lines of evidence, including zero reaction order in MNQ, rate-accelerating effect of base, detection of acetamide in the reaction mixture, negligible reaction rate in ethyl acetate, and recognition of weak basic sites in the niobium silicates using infrared spectroscopy of adsorbed CDCl₃, all indicate that MNQ epoxidation proceeds by another mechanism that involves rate-limiting oxidation of the solvent molecule (MeCN) to generate peroxy-carboximidic acid, which reacts with electron-deficient C=C bonds, producing an epoxy derivative and acetamide.

© 2017 Elsevier Inc. All rights reserved.

1. Introduction

Alkene epoxidation is one of the most important transformations in the manufacture of bulk and fine chemicals/intermediates [1,2]. Traditionally, epoxidation in organic synthesis is accomplished through oxidation with organic peracids or by the chlorohydrin route. Since these approaches are not environmentally benign, great scientific effort has been directed to the development of effective catalytic methods for epoxidation using aqueous hydrogen peroxide as a green oxidant, which produces water as the sole byproduct [3–7]. The discovery of titanium silicalite-1 (TS-1) by Eni researchers has become one of the major break-

throughs in the field of heterogeneous liquid-phase oxidation with H₂O₂ [8–10]. However, the scope of application of TS-1 is limited to oxidation of relatively small organic substrates, which are able to penetrate into the micropores of this catalyst. A range of mesoporous titanium silicates have been developed, but most of them suffer from the gradual aggregation of Ti sites while using aqueous H₂O₂ as oxidant and are selective only with electron-rich olefins containing no allylic hydrogen atoms [11,12]. Therefore, the quest for catalysts that would be both effective in activation of H₂O₂ and broad in scope remains a challenging goal of oxidation catalysis.

In recent years, niobium-containing catalysts have attracted growing interest in the selective oxidation community. Mesoporous niobium silicates prepared by different methodologies turned out to be active and recyclable catalysts for epoxidation of various olefins using aqueous hydrogen peroxide as oxidant [13–30]. In general, these catalysts reveal higher epoxidation selec-

* Corresponding author at: Borekov Institute of Catalysis, Lavrentieva Avenue 5, Novosibirsk 630090, Russia.

E-mail address: khold@catalysis.ru (O.A. Kholdeeva).

tivity than mesoporous titanium catalysts [21,30], and in addition, they are able to epoxidize electron-deficient C=C bonds in α,β -unsaturated carbonyl compounds [24,29]. Another interesting feature of the Nb catalysts is unusual regioselectivity toward epoxidation of the less electron-rich exocyclic C=C bond in terpenes [21,24]. Recently, Ivanchikova et al. have demonstrated that the crucial factor that governs the rate and regioselectivity of limonene epoxidation over mesoporous niobium silicates is the nature of the solvent [29]; the highest ratio of exo/endo epoxides was obtained in acetonitrile. Hence, the catalytic performance of mesoporous niobium catalysts differs markedly from that of their Ti counterparts. Isolated and undercoordinated Nb(V) species were assumed to be responsible for the high catalytic activity of niobium silicates in selective oxidation with hydrogen peroxide [13,15,21,23,27,28,31,32]. The presence of Nb₂O₅-like nanoaggregates was detrimental to the catalytic performance [23,24]. Recently, a direct comparison of the behavior of catalysts with site-isolated and evenly dispersed di(oligo)meric Nb centers at similar Nb loadings has shown that both types of catalysts are able to accomplish epoxidation of both electron-rich and electron-deficient C=C bonds [29]. Catalysts with predominately isolated Nb centers were preferable for the selective formation of epoxides sensitive to ring-opening and overoxidation, whereas single-site and (di)oligomeric Nb sites were equally effective for the production of relatively stable epoxides [29]. While high levels of understanding have been achieved in the areas of epoxidation over Ti, V, Mo, W, and Re catalysts [10,11,33–35], as well as biomimetic catalysts based on Fe and Mn [33,36,37], epoxidation over Nb is still poorly understood. So far, few research groups have attempted to rationalize the catalytic activity of niobium in H₂O₂-based oxidation [30–32,38–40]. Detailed mechanistic information, in particular provided by kinetic and spectroscopic studies, is still limited, although it is crucial for understanding the factors that control catalytic performance.

In this work, we have studied the kinetics of H₂O₂-based Nb-catalyzed epoxidation using two model substrates, cyclooctene (CyO, electron-rich C=C bond) and 2-methyl-1,4-naphthoquinone (MNQ, electron-deficient C=C bond), and two mesoporous niobium silicate catalysts that contained predominantly site-isolated or di(oligo)meric Nb(V) and were prepared by the same evaporation-induced self-assembly (EISA) methodology using different Nb precursors. The results of the kinetics study, coupled with additive and solvent effects, implied different mechanisms for epoxidation of electron-rich and electron-deficient C=C bonds over Nb(V). Diffuse reflectance (DR) UV–vis spectroscopic study was employed to probe peroxo niobium species formed upon interaction with H₂O₂. To understand better the difference in the catalytic performance of mesoporous Nb and Ti silicates, we also performed a comparative study of H₂O₂ decomposition and explored the acid–base surface properties of these catalysts by means of FTIR spectroscopy of adsorbed probe molecules (pyridine (Py), CO, and CDCl₃).

2. Experimental

2.1. Materials and catalysts

Cetyltrimethylammonium bromide (CTAB, 99%+), tetraethyl orthosilicate (TEOS, 98%+), and ammonium niobate(V) oxalate hydrate NH₄[NbO(C₂O₄)₂(H₂O)₂] \cdot 3H₂O (99.99%) were purchased from Aldrich. Niobium(V) ethoxide (99.95%) was used as received from Acros. Acetonitrile (HPLC grade, Panreac) was dried and stored over activated 4 Å molecular sieves. Cyclohexene and *cis*-cyclooctene were purchased from Aldrich and passed through a column filled with neutral alumina before use. All other reagents

and solvents were the best reagent grade and were used without further purification. The concentration of H₂O₂ (30% in water) was determined iodometrically prior to use. Deionized water (EASY pure, RF, Barnsted) was used for the preparation of catalysts.

Mesoporous niobium silicates containing mainly di(oligo)meric (catalyst A) or isolated (catalyst B) Nb(V) sites were prepared by the EISA technique using niobium(V) ethoxide and ammonium niobate(V) oxalate hydrate, respectively [29]. For comparison, a mesoporous titanium silicate with oligomeric Ti(IV) sites (catalyst A-Ti) was prepared by the same EISA approach, following a protocol reported previously [41]. The catalysts were characterized by elemental analysis, low-temperature N₂ adsorption, FTIR, and DR UV–vis techniques.

2.2. Infrared with adsorption of probe molecules

FTIR spectra were recorded on a Shimadzu FTIR 8300 spectrometer with a resolution of 4 cm⁻¹, accumulating 200 scans. The catalysts were pressed into thin wafers (12–25 mg/cm²) and calcined directly in the IR cell at 450 °C in vacuum for 1 h. The spectra were normalized to the wafer weight and presented in arbitrary units. Pyridine was adsorbed at 180 °C for 15 min and then evacuated at the same temperature for 30 min. The IR spectra were measured at room temperature. CO was adsorbed at 77 K by several portions at equilibrium pressures of 0.1, 0.4, 0.9, and 1.5 Torr. The IR spectra were recorded at 77 K. CDCl₃ was adsorbed at room temperature by injecting a portion of 2000 μ mol/g into the cell, and the spectra were measured immediately after injection. A reference spectrum of the corresponding catalyst run at the measurement temperature was subtracted. Concentrations of acidic and basic sites were estimated from integral intensities of the characteristic IR bands. The number of Brønsted acid sites (BAS) was evaluated from the band at 1530–1550 cm⁻¹ (PyH⁺ ions) using a molar absorption coefficient ϵ equal to 3 cm²/mol (in the literature, ϵ_{1545} usually varies from 1.25 to 3 cm²/mol [42–47]; 3 cm²/mol was measured for solid PyHCl salt [47]). The number of Lewis acid sites (LAS) was estimated from the band at 1450 cm⁻¹ (coordinatively bonded Py) after deconvolution of the band at 1445–1455 cm⁻¹, using $\epsilon_{1450} = 3.5$ cm²/mol (typical values reported in the literature are in the range 1.73–3.5 cm²/mol [42,43,45,46]). The concentrations of BAS and LAS were also assessed from the intensity of CO bands at 2162–2170 and 2183–2195 cm⁻¹ using ϵ of 2.6 and 0.9 cm²/mol, respectively [46]. The error in measuring the amounts of BAS and LAS was 20–30%. The strength of LAS was assessed on a scale of CO adsorption heat according to the equation Q [kJ/mol] = 10.5 + 0.5 Δv_{CO} , where $\Delta v_{CO} = v_{CO(ads)} - 2143$ [46]. The strength of BAS in terms of proton affinity (PA) was evaluated from the shift of the absorbance bands in the O–H stretching region due to their interaction with CO using the equation PA [kJ/mol] = 1390 – log($\Delta v_{OH}/\Delta v_{OH(SiOH)}$)/0.00226, where Δv_{OH} and $\Delta v_{OH(SiOH)}$ are shifts of O–H vibration frequencies in the solid studied and SiO₂, respectively ($\Delta v_{OH(SiOH)}$ was taken as 90 cm⁻¹) [46]. The uncertainty in estimating the strength of BAS and LAS did not exceed 2–3%. Concentrations of basic sites were estimated using a molar absorption coefficient (0.16 cm²/mol) reported in the literature for CDCl₃ complexes with different bases [46,47]. The error in measuring the number of basic sites was within 20%. The strength of basic sites was evaluated from the shift of the C–D stretching band according to the equation log $\Delta v_{CD} = 0.0066 \times PA - 4.36$, where $\Delta v_{CD} = 2268 - v_{CD(ads)}$ [47,48]. The error in estimating the strength of basic sites was 2%.

2.3. Kinetic experiments

Kinetic experiments were performed in temperature-controlled glass vessels under vigorous stirring (600 rpm). Reactions were ini-

tiated by addition of H₂O₂ into a MeCN solution containing organic substrate (CyO or MNQ), a catalyst, and an internal standard for GC. The total volume of the reaction mixture was 1 mL. The reaction temperature was 50 °C for CyO and 70 °C for MNQ. Typical reaction time was 1–2 h for CyO and 2–6 h for MNQ. Samples (1 μL) of the reaction mixture were withdrawn periodically during the reaction with a syringe and analyzed. Substrate conversions and epoxide product yields were quantified using biphenyl as internal standard. Each experiment was reproduced at least 2–3 times. To rule out the possibility of evaporative losses of the substrate, blank experiments without catalyst and oxidant were carried out at the reaction temperature using the internal standard.

2.3.1. Reaction order in catalyst

The catalyst amount was varied in the range 7.5–45 mg, which corresponds to 0.0015–0.009 mmol of Nb. Concentrations of other reactants were held constant: substrate 0.1 M, H₂O₂ 0.1 (CyO) or 0.4 M (MNQ).

2.3.2. Reaction order in substrate

The initial substrate concentration was varied between 0.01 and 0.2 M while maintaining a constant concentration of H₂O₂ (0.1 and 0.4 M for CyO and MNQ, respectively) and catalyst amount (0.015 g; 0.003 mmol Nb).

2.3.3. Reaction order in H₂O₂

The initial oxidant concentration was varied in the range 0.05–0.4 M (for CyO) or 0.1–0.8 M (MNQ). The concentration of water in these experiments was kept constant by addition of corresponding amounts of H₂O. The concentrations of other reactants were as follows: CyO or MNQ 0.1 M, catalyst 0.015 g (0.003 mmol Nb).

2.3.4. Reaction order in H₂O

The initial concentration of water was varied from 0.2 to 1.7 M (CyO) and from 0.8 to 3.1 M (MNQ). Other parameters were held constant: substrate 0.1 M, catalyst 0.015 g (0.003 mmol Nb), H₂O₂ 0.1 M (CyO) or 0.4 M (MNQ).

2.3.5. Determination of activation energies

Temperature dependence of the reaction rate was studied in the range 30–80 °C in MeCN using the following reaction conditions: CyO or MNQ 0.1 M, H₂O₂ 0.1 or 0.4 M for CyO or MNQ, respectively, and 0.015 g catalyst (0.003 mmol Nb).

2.4. Initial rate determination and evaluation of rate laws

The initial rate method was employed to determine the reaction orders. Initial rates were calculated as $d[\text{CyO}(\text{or MNQ})]/dt$ at $t = 0$. Since epoxides were the sole products at low conversion, the initial reaction rates of substrate consumption and epoxide accumulation were close to each other. The rate law was derived by applying a steady-state approximation to concentrations of all active species. Procedures for calculating the initial rates and fitting the rates with the derived law were similar to those described by some of us earlier [49]. For the detailed description of the kinetic modeling procedure and derivation of the rate law, see the [Supporting Information \(SI\)](#).

2.5. Effects of additives

Acid (HClO₄) or base (NaOAc) was added into the reaction mixtures before addition of the oxidant in an amount close to the amount of Nb in the catalyst loaded (0.003 mmol). Turnover frequencies (TOF) were determined from the initial rates and calculated as TOF = (moles of substrate consumed)/(moles of Nb × time).

2.6. Stereospecificity tests

Oxidation of *cis*-/*trans*-stilbenes and *cis*-β-methylstyrene was carried out at 50 °C in MeCN (1 mL) using the following concentrations of the reagents: alkene 0.1 M, H₂O₂ 0.1 M, and catalyst 0.003 mmol Nb. The ratio of *cis*- and *trans*-epoxides was determined by ¹H NMR and GC–MS techniques.

2.7. Oxidation of cyclohexene

Catalytic oxidation of cyclohexene was carried out at 30 and 50 °C in MeCN (1 mL) using the following concentrations of the reagents: CyH 0.1 M, H₂O₂ 0.1 M (taken as a 50% solution in water), and 0.003 mmol Nb or Ti catalyst. The product yields and substrate conversions were quantified by GC using biphenyl as an internal standard. For GC analysis, we used the method described by Shul'pin [50], which is based on treatment of the reaction mixture with triphenylphosphine to reduce unreacted H₂O₂ and cyclohexenyl hydroperoxide formed during the reaction.

2.8. Hydrogen peroxide decomposition

Decomposition of H₂O₂ (0.4 M) was studied in the absence of organic substrate at 80 °C in MeCN (5 mL) in the presence of either Nb or Ti catalyst (0.015 mmol Nb or Ti). Aliquots of 0.2 mL were taken during the reaction course, and H₂O₂ concentration was determined by iodometric titration. Four parallel experiments were carried out. The temperature dependence of the decomposition rate was studied in the range 40–80 °C.

2.9. DR UV–vis study of H₂O₂ interaction with Nb catalyst

Catalyst **B** (0.57 g, 0.11 mmol Nb) was placed in a mixture of MeCN (6 mL) and 30% H₂O₂ (2 mL), and the slurry was stirred at room temperature for 15 min. Then the catalyst was separated by filtration and divided into two portions. The first portion was treated with H₂O (5 mL) to remove physisorbed H₂O₂, while the second was subjected to treatment with an aqueous solution of NaOAc (5 mL, 0.16 mmol) for 15 min at room temperature. The catalyst was separated by filtration under vacuum, dried in air and used for DR UV–vis measurements.

2.10. Instrumentation

GC analyses were performed using a Chromos GH-1000 gas chromatograph equipped with a flame ionization detector and a quartz capillary column (30 m × 0.25 mm) filled with BP-5. Substrate conversions and product yields in all cases were determined by the internal standard technique. GC–MS analyses were carried out using an Agilent 7000 GC/MS system equipped with a CM-WAX fused silica capillary column (10 m × 0.25 mm × 0.25 μm). The mass spectrometer worked in EI mode at 70 eV, scan range 40–550 *m/z*. The identification of components was based on computer matching of their mass spectra with those of the NIST11 mass spectral library (NIST MS Search 2.0, 2005). Nitrogen adsorption measurements were performed at 77 K using a NOVA 1200 instrument (Quantachrome) within the partial pressure range 10^{−4}–1.0. The catalysts were degassed at 150 °C for 24 h before the measurements. Surface areas were determined by the BET analysis. Pore size distributions were calculated from the adsorption branches of the nitrogen isotherms by the regularization procedure, using reference local isotherms calculated for a cylindrical silica pore model in the framework of the density functional theory (DFT) approach. Special software provided by Quantachrome Corp. was used. Mean pore diameters were calculated as mathematical expectation values from the pore size distributions. Niobium con-

tent in the solids was determined by ICP–AES using a Thermo Scientific iCAP–6500 instrument. The state of niobium in the catalysts was characterized by DR UV–vis spectroscopy under ambient conditions using a Shimadzu UV–VIS 2501PC spectrometer in the 190–900 nm range with a resolution of 2 nm; BaSO₄ was used as standard reference. The infrared (IR) spectra were recorded on a Shimadzu FTIR 8300 spectrometer.

3. Results and discussion

3.1. Catalyst preparation and characterization

In our previous studies, we demonstrated that EISA is an affordable and versatile method for the preparation of hydrothermally stable and leaching-tolerant mesoporous titanium [41] and niobium silicates [29] with a weakly ordered structure. This method enables easy control of the state of Nb active centers and, depending on the choice of the niobium precursor, favors the formation of either small oligomers (type **A**) or site-isolated Nb(V) species (type **B**) [29]. Using the EISA approach, we synthesized niobium silicates of these two types (hereinafter, catalysts **A** and **B**) and used them for exploring kinetic regularities of CyO and MNQ epoxidation with H₂O₂. For comparison, we also prepared a mesoporous titanium silicate (designated as catalyst **A-Ti**) by the EISA method. All three catalysts had similar textural properties and metal content (Table 1). A complete characterization of these catalysts by XRD, SEM, N₂ adsorption, and spectroscopic techniques (DR UV–vis, Raman, and XPS) has been reported elsewhere [29,41]. DR UV–vis spectra of catalysts **A**, **B**, and **A-Ti** are shown in Fig. S1.

3.2. FTIR study of surface acid–base properties

Infrared spectroscopy permits discrimination between various types of surface sites based on the effects on the spectral features of the adsorbed probe molecules induced by acid–base interaction [46,51]. Several IR studies employing probe molecules (Py, CD₃CN, NO) revealed Lewis acid sites (LAS) in dehydrated Nb-containing molecular sieves [40,52–56]. Only one type of LAS was identified by adsorption of CD₃CN onto Nb-β [40]. Brønsted acid sites (BAS) are not present in this zeolite, as shown by Py [53] and CD₃CN [40] adsorption. On the other hand, BAS appeared in niobium-rich mesostructured materials (Nb-SBA-15 [52] and Nb-KIT-6

[54]), mixed oxides [32], and supported niobium oxides [57], but their number remained lower relative to the number of LAS. So far, very few experimental studies have dealt with evaluation of basic sites in Nb-containing silica materials. On the basis of ESR, NO/FTIR, and catalytic studies, Ziolek and co-workers suggested that Lewis acidic and basic sites appear simultaneously in the Nb-containing molecular sieves upon dehydration [55,56]. The total acidity and basicity, evaluated by temperature-programmed desorption (TPD) of Py and CO₂, respectively, were found to be close in Nb-KIT-6 and increased with enlarging Nb loading [58]. In this work, we employed FTIR spectroscopy of weakly (CO) and strongly (Py) interacting bases to probe semiquantitatively the number and strength of LAS and BAS in mesoporous niobium silicates **A** and **B** in comparison with titanium silicate **A-Ti** prepared by the same method. In addition, adsorption of CDCl₃ was used to estimate the number and strength of basic sites. Fig. S2 shows FTIR spectra of Py adsorbed at 423 K on the three catalysts studied. The band at 1530–1550 cm⁻¹ corresponding to PyH⁺ ions [43–46] is present in the spectra of both Nb catalysts but is missing in the spectrum of the Ti catalyst. The number of BAS is larger for catalyst **A** with oligomeric Nb sites, which agrees with the literature [32,52,54,57]. The bands at 1607–1610 cm⁻¹ (ν_{8a}) are attributed to complexes of Py with LAS (PyL), while the band at 1600 cm⁻¹ (ν_{8a}) corresponds to H-bonded Py [43,44,46]. The absorption feature at 1448 cm⁻¹ (ν_{19b}) is observed as a result of overlapping bands of coordinatively bonded (1450 cm⁻¹) and H-bonded (1440 cm⁻¹) Py. The concentrations of BAS and LAS estimated from the intensity of the characteristic bands at 1545 and 1450 cm⁻¹, respectively, are given in Table 2.

One of the most reliable and informative approaches to exploring BAS and LAS in heterogeneous catalysts is adsorption of weakly interacting probe molecules, e.g., CO at 77 K, monitored by IR spectroscopy [46,51,59]. The spectra of CO adsorbed onto catalyst **A** at different pressures are shown in Fig. 1. A similar picture was observed for catalyst **B** (Fig. S3). At low CO pressure, two bands at 2163 and 2193 cm⁻¹ are present. The first can be attributed to CO interacting with surface BAS through H-bonding, while the second corresponds to CO coordinatively bonded to LAS [46,59]. With increasing CO pressure, the band at 2193 cm⁻¹ shifts to 2191 cm⁻¹ and its intensity increases. Simultaneously, a new absorption feature at 2157 cm⁻¹ arises on the left side of the 2163 cm⁻¹ band and increases in intensity. This band is due to CO molecules H-bonded to silanol groups [46,59]. Therefore, two types of BAS can be distinguished in the niobium silicates. The IR spectra of CO adsorbed onto catalyst **A-Ti** (Fig. S4) are similar to the corresponding spectra reported earlier for titanium silicates prepared by different methods [59] and reveal only two characteristic bands, at 2157 and 2186 cm⁻¹ (the latter shifts to 2183 cm⁻¹ at high CO pressure), which indicates that BAS different in strengths from SiOH groups are absent.

The concentrations of BAS and LAS determined from the intensity of the CO bands at 2162–2170 and 2183–2195 cm⁻¹, respectively, are provided in Table 2. The values acquired using Py and CO probe molecules are in good agreement, which implies fairly

Table 1
Metal content and textural characteristics of Nb and Ti silicates.

Catalyst	M, wt.% ^a	S _{BET} , m ² /g	V _p , cm ³ /g ^b	D _p , nm ^c
A	1.96	1190	0.56	2.8
B	1.80	1280	0.57	2.8
A-Ti	2.35	1270	0.54	2.7

^a Based on elemental analysis data for calcined samples.

^b Mesopore volume.

^c Mean pore diameter.

Table 2
Acidity and basicity of Nb- and Ti-containing silicates.^a

Catalyst	Brønsted acid sites			Lewis acid sites			Basic sites	
	Py		N, μmol/g	CO		N, μmol/g	CDCl ₃	
	N, μmol/g	PA, kJ/mol		N, μmol/g	Q, kJ/mol		N, μmol/g	PA, kJ/mol
A	12	1200	12	33	36	32	780	760
B	5	1200	10	21	35	23	780	520
A-Ti	<2	–	<1	12	32	15	740	640

^a See Section 2.2 for calculation details and measurement errors.

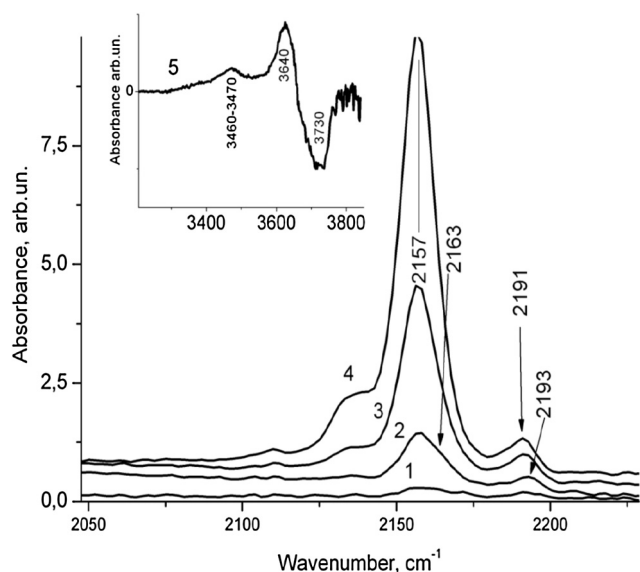


Fig. 1. FTIR spectra of CO adsorbed at 77 K on catalyst **A** (carbonyl stretching region): (1) CO pressure 0.1 Torr, (2) 0.4 Torr, (3) 0.9 Torr, and (4) 1.5 Torr. In the insert: (5) spectrum of O–H stretching region measured after CO adsorption at 0.4 Torr. The spectrum of catalyst **A** before interaction with adsorbate molecules was used for background subtraction.

good accessibility of the Nb sites in both catalysts. Similarly to other Nb-containing silica materials [52,54,57,58], the number of LAS is significantly larger than the number of BAS. One can notice that the concentration of LAS seems underestimated relative to the number of Nb sites calculated on the basis of the elemental analysis data (ca. 200 $\mu\text{mol/g}$). The reason for that could be uncertainty in the molar extinction coefficient ϵ , which depends on the particular adsorbate and adsorbent [51,59]. Since the true value of ϵ for the mesoporous Nb and Ti silicates is unknown, the values determined for the bulk oxides were used in the calculations (see Section 2.2), which could lead to underestimation of the number of LAS. Nevertheless, a rough estimate and comparison of the number of sites within a series of catalysts can be used to assess their relative accessibility [59]. Since the concentration of LAS seems to be close for catalysts **A** and **B** within experimental error, which is 20–30%, we may infer that Nb sites possess similar accessibility in both Nb catalysts. This can be envisioned if catalyst **A** contains evenly dispersed coordinatively unsaturated dimers or small oligomers of Nb(V); otherwise the number of LAS would be expected to decrease relative to the number in catalyst **B**, which has mostly site-isolated Nb.

Although quantitative determination of acid or base strength appears to be extremely difficult, relative sequences of these quantities for comparable groups of solid catalysts can be established [51]. The strength of BAS can be evaluated from the shift of the absorbance band in the O–H stretching region caused by the interaction with probe molecules, such as CO or MeCN [32,46,51,59]. The insert in Fig. 1 shows a difference spectrum of this region measured for catalyst **A**. While the band at 3640 cm^{-1} is due to SiOH groups H-bonded with CO, the broad band at 3460–3470 cm^{-1} can be assigned to BAS associated with Nb [46]. The values of proton affinity (PA) estimated for BAS on the basis of the band shift relative to the frequency of the O–H stretching before CO adsorption are presented in Table 2. The band shift $\Delta\nu_{\text{OH}}$ of ca. 270 cm^{-1} and the corresponding value of PA (1200 kJ/mol) indicate that BAS in the niobium silicates are of moderate strength. This is consistent with the conclusions made for other Nb–silica catalysts on the basis of studies by NH_3 TPD [54] and FTIR with adsorbed MeCN [32]. The strength of BAS in Nb catalysts is significantly higher than

in Ti catalysts, for which typical values of $\Delta\nu_{\text{OH}}$ lie in the range 90–100 cm^{-1} and are close to the $\Delta\nu_{\text{OH}}$ established for silica [59]. Also, the strength of LAS assessed on the scale of CO adsorption heat [46] (Table 2) turned out to be higher for the Nb catalysts than for the Ti one. On the other hand, the strength of LAS for the Nb catalysts **A** and **B** is approximately the same within experimental error (2–3%).

The number and strength of basic sites were assessed using CDCl_3 as a probe molecule [46]. This method was first suggested by Paukshtis and co-workers [60] and then employed by other researchers in exploring basic sites in heterogeneous catalysts [48,51]. The IR spectra of adsorbed CDCl_3 are presented in Fig. S4. The broad band centered at 2262 (catalysts **A** and **B**) cm^{-1} corresponds to C–D stretching vibration of CDCl_3 adsorbed onto weak basic sites [46,60]. Previously, weak basic sites were identified in Nb_2O_5 oxide by IR spectroscopy using CHCl_3 as a probe molecule ($\Delta\nu_{\text{CH}}$ 13 versus 38 cm^{-1} for Al_2O_3 [45]). For catalyst **A**-Ti, the value of ν_{CD} is very close to that measured for CDCl_3 adsorbed on silica (2265 cm^{-1}) [48,60]. Estimates of the number of basic sites and their strength in terms of PA are provided in Table 2. Three main conclusions can be drawn from these data: (1) the difference in PA between **A** and **A**-Ti (780 versus 740 kJ/mol) is outside the uncertainty of the measurements and indicates that weak basic sites are present in the Nb silicates and absent in the Ti silicate (PA 733 kJ/mol was reported for SiO_2 [48]); (2) among the Nb silicates, the number of weak basic sites is larger for catalyst **A**, which contains di(oligo)meric Nb sites; and (3) the estimated concentrations of basic sites are of the same order of magnitude as the general number of Nb–O–Nb/Nb–O–Si bonds in the Nb silicates calculated on the basis of the elemental analysis data under the assumption that one Nb(V) is surrounded by four bridging oxygen atoms along with one terminal oxygen (=O or –OH).

Subramaniam and co-workers demonstrated that the total acidity and basicity increase with increasing niobium loading in Nb-KIT-6 [58]. This agrees with our finding that the number of both BAS and basic sites is larger in catalyst **A** than in catalyst **B**.

3.3. General features of epoxidation kinetics

The epoxides derived from CyO and MNQ possess fairly good stability toward epoxide ring opening and rearrangement, which results in excellent epoxidation selectivity in H_2O_2 -based oxidation over the Nb catalysts (both **A** and **B**) [29]. For this reason, these two compounds were chosen as model substrates for kinetic studies. Previously, we demonstrated by a hot filtration test and elemental analysis data [61] that oxidation catalysis over Nb silicates prepared by EISA has a truly heterogeneous nature and there is no niobium leaching [29]. For both substrates, the reaction rate was negligible in the absence of catalyst or oxidant. Kinetic plots for CyO and MNQ consumption over catalysts **A** and **B** revealed no induction period over the entire range of concentrations used. The initial epoxidation rates and epoxide yields were not affected by light, which ruled out any photochemical process over the niobium silicates. Kinetic curves acquired under Ar and in air coincided completely, indicating that molecular oxygen is not involved, at least in the rate-limiting step of the oxidation reactions. Addition of the conventional radical scavenger ionol produced no rate-retarding effect. All these facts collectively imply a nonradical oxidation mechanism or a mechanism with short radical chains.

The reaction rates were not affected by the rate of stirring of the reaction mixture in the range of 500–1000 rpm, showing that external diffusion of reactants to catalyst particles does not limit the overall oxidation rate. In line with this, epoxidation rates were proportional to the catalyst loading. Surprisingly, kinetic regularities did not depend on the state of Nb centers (isolated or

oligomerized) but were solely determined by the nature of the organic substrate (*vide infra*).

3.4. Kinetics of CyO epoxidation

Fig. 2 shows the dependence of initial rates of CyO consumption on concentrations of alkene, hydrogen peroxide, niobium, and water. Notwithstanding the type of catalyst (A or B), the epoxida-

tion rate exhibited saturation with increasing concentrations of alkene (Fig. 2a) and oxidant (Fig. 2b) and increased proportionally to the catalyst loading (Fig. 2c). The reaction was mildly inhibited by H₂O (Fig. 2d). In contrast to epoxidation over the microporous zeolite Nb-β, where the rate of epoxidation depended inversely on the C₆H₁₀O concentration [40], addition of CyO epoxide (ca. 40 mol.% of the amount of alkene) did not affect the reaction rate,

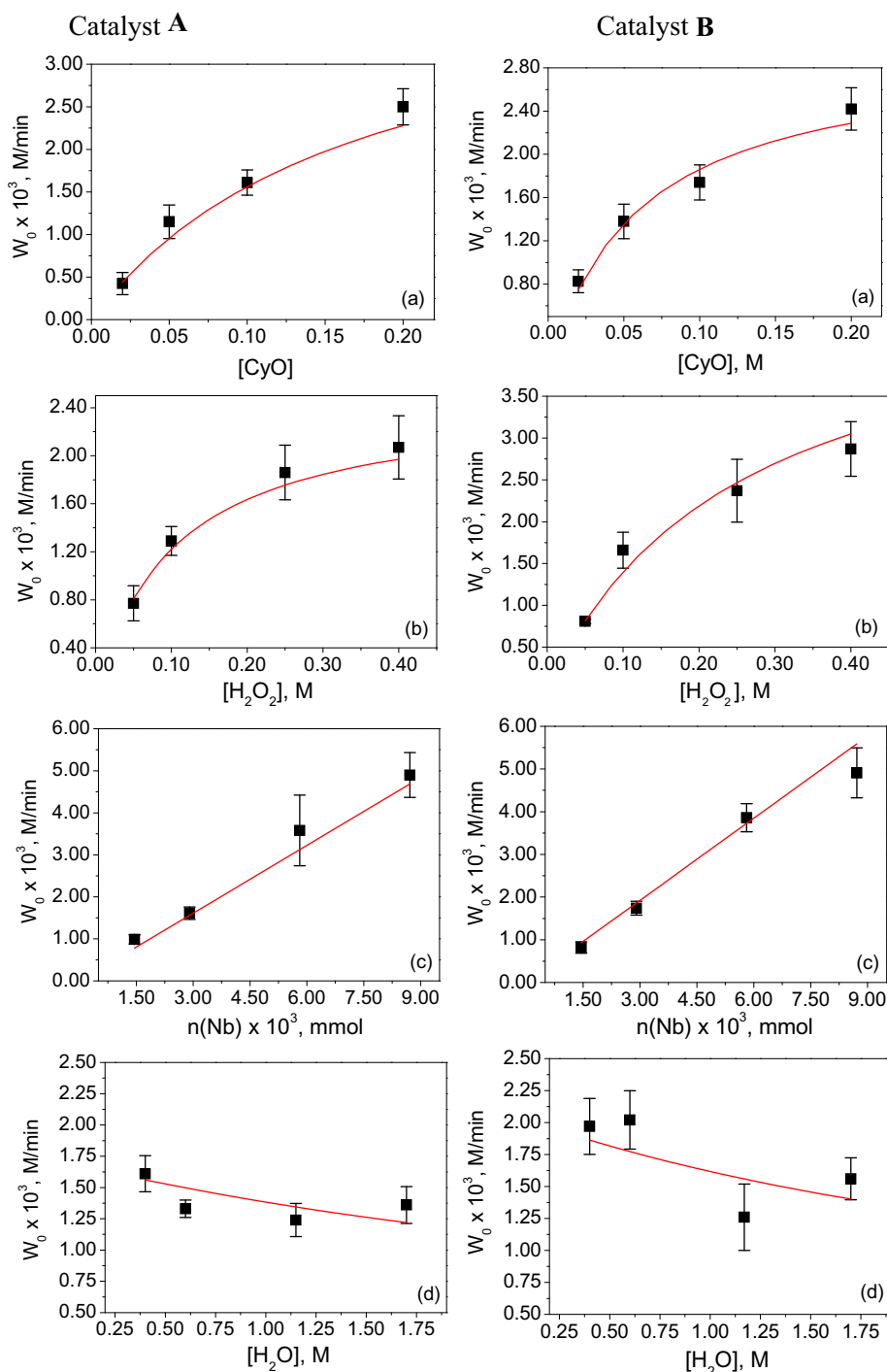


Fig. 2. Plots of the initial rate of CyO oxidation (MeCN, 50 °C) versus concentration of alkene (a), oxidant (b), catalyst (c), and water (d): experimental points (■) and fitting (—) to an equation given in Section 3.9. For other reaction conditions, see Section 2.3.

thereby indicating that adsorption of the main oxidation product onto the mesoporous Nb catalyst is insignificant.

The rate of CyO oxidation exhibited a typical Arrhenius dependence, which implies that there is no change in the rate-limiting step in the temperature interval used. The values of the apparent activation energy (E_a) for catalysts **A** and **B** estimated from the Arrhenius plots (Fig. 3) are close, 11.9 and 10.9 kcal/mol, respectively. Earlier, an activation energy of 10.3 kcal/mol was reported for epoxidation of styrene over a mesoporous catalyst Nb-KIT-5 [27]. Note that such values of E_a are typical of reactions controlled by chemical interaction, because for reactions controlled by diffusion processes, E_a is expected to be <4 kcal/mol [62].

As one can judge from the plots shown in Fig. 3, the rate of CyO epoxidation was always a little higher for catalyst **B** than catalyst **A**, which seems reasonable taking into account greater isolation of Nb sites in the former.

3.5. Hydrogen peroxide decomposition

Unproductive decomposition of hydrogen peroxide is the main reaction that competes for H_2O_2 with the target selective oxidation reaction [26,29,63,64]. Taking this into account, we evaluated the activity of catalysts **A** and **B** in H_2O_2 decomposition in the absence of any organic substrate. Fig. 4 shows kinetic plots of H_2O_2 decay over two niobium silicates and titanium silicate of type **A** (the amount of Nb or Ti was similar in all the experiments). No H_2O_2 conversion occurred in the absence of any catalyst.

Among the Nb silicates, catalyst **B** was a bit more active than catalyst **A** (TOF 1.05 versus 0.85 min^{-1}). More important is that both Nb catalysts are significantly less active in this reaction than the Ti catalyst prepared by the same EISA technique (TOF 3.3 min^{-1}). This agrees with the smaller amounts of homolytic oxidation products formed from substrates with reactive allylic H atoms (e.g., cyclohexene and limonene) over niobium silicates than over their Ti analogues [21,30] (see also Section 3.6). It is generally believed that acid sites of moderate strength are involved in the mechanism of epoxidation of alkenes with H_2O_2 , while strong acidity activates the decomposition of H_2O_2 [32]. The results of the FTIR spectroscopic study presented in Table 2 allow one to conclude that the difference in the H_2O_2 decomposition rates observed for the Nb and Ti catalysts is certainly not related to the difference in their Brønsted acidity, which decreases in the order **A** > **B** > **A**-Ti. We may assume that higher activity of the Ti silicate in H_2O_2 decomposition can be related to lower energy cost of homolytic

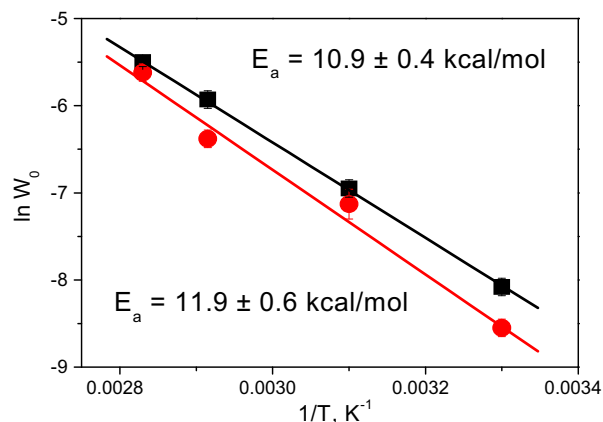


Fig. 3. Arrhenius plots for CyO oxidation over catalysts **A** (●) and **B** (■). Reaction conditions: CyO 0.1 M, H_2O_2 0.1 M, catalyst 0.003 mmol Nb, MeCN 1 mL, 30–80 °C.

O—O bond breaking in the hydroperoxo intermediate, similarly to that in homogeneous Ti-containing polyoxometalates [35].

Activation energies of H_2O_2 decomposition over catalysts **A** and **B** were determined from the Arrhenius plots shown in Fig. 5.

It is noteworthy that the apparent activation energies for CyO epoxidation are significantly lower than the E_a established for decomposition of H_2O_2 : 11.9 vs. 20.5 kcal/mol for catalyst **A** and 10.9 vs 16.6 kcal/mol for catalyst **B**. Therefore, one might expect that epoxidation selectivity (or, in case of epoxides sensitive to ring opening, total selectivity to epoxide, diol, and their overoxidation products) might be improved by decreasing the reaction temperature. To verify this suggestion, we have studied the effect of temperature on the selectivity of cyclohexene oxidation.

3.6. Effect of temperature on epoxidation of cyclohexene

The data presented in Table 3 show that the total heterolytic pathway selectivity (we define it as the sum of epoxide, *trans*-cyclohexane-1,2-diol, and 2-hydroxycyclohexane-1-one) increased from 70–71% to 85–88% at similar alkene conversions when the reaction temperature was reduced from 50 to 30 °C. This effect was less pronounced for the titanium catalyst **A**-Ti.

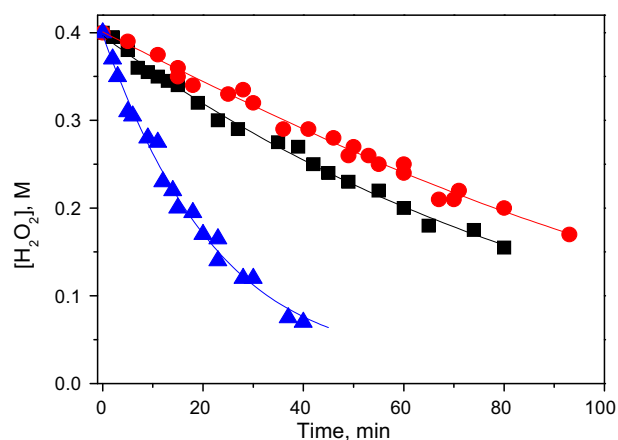


Fig. 4. H_2O_2 decomposition in the absence of organic substrate over catalysts **A** (●), **B** (■), and **A**-Ti (▲). Reaction conditions: H_2O_2 0.4 M, catalyst 0.015 mmol Nb or Ti, 80 °C, MeCN 5 mL. Points acquired from four parallel experiments are shown for each curve.

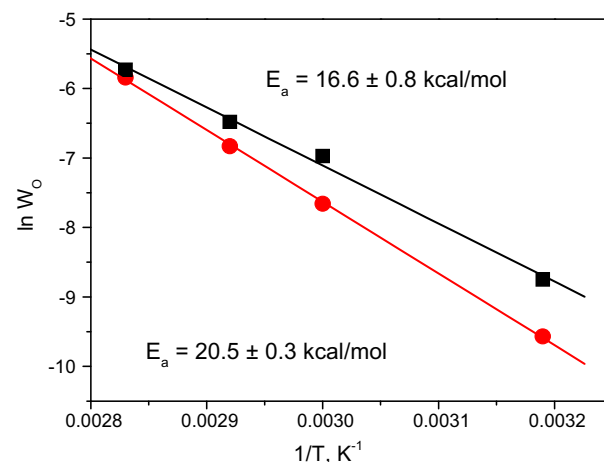


Fig. 5. Arrhenius plots for H_2O_2 decomposition over catalysts **A** (●) and **B** (■). Reaction conditions: H_2O_2 0.4 M, Nb 0.02 mmol, MeCN 7 mL, 40–80 °C.

Table 3
Effect of temperature on selectivity of CyH oxidation over Nb and Ti catalysts.

Catalyst	T, °C	Time, h	CyH conv., %	Heterolytic pathway selectivity, % ^a	Homolytic pathway selectivity, % ^b
A	30	1	23	85	11
B	30	1	30	88	9
A-Ti	30	2	24	70	21
A	50	0.5	30	70	18
B	50	0.3	34	71	21
A-Ti	50	2.5	35	65	27

Note: Reaction conditions: CyH 0.1 mmol, 50% H₂O₂ 0.1 mmol, catalyst 0.003 mmol Nb or Ti, MeCN 1 mL.

^a Total selectivity of heterolytic oxidation products (cyclohexene oxide + *trans*-cyclohexane-1,2-diol + 2-hydroxycyclohexanone).

^b Total selectivity of homolytic oxidation products (cyclohexenyl hydroperoxide + 2-cyclohexene-1-ol + 2-cyclohexene-1-one).

Interestingly, an opposite trend was predicted for zeolite Nb-β, for which the activation enthalpy appeared to be significantly higher for cyclohexene epoxidation than for H₂O₂ decomposition (17.2 vs 10.8 kcal/mol) and therefore improvement of selectivity was expected with rising reaction temperature [40]. Unfortunately, no data on product selectivity at different temperatures were provided to verify this prediction.

3.7. Presumably active species: Heterolytic vs. homolytic mechanism of alkene epoxidation

Various oxidizing species were proposed as active forms responsible for liquid-phase selective oxidation over heterogeneous niobium catalysts. Among them were both radical forms, including HO• [39], superoxo Nb^VO₂⁻ [38] and Nb^{IV}-(O₂)⁻ [40], and a species designated as Nb-O⁻ [55,56], and nonradical forms, such as side-on peroxo Nb(η²-O₂) [65,66] and end-on hydroperoxo [14,31,32] species. Various structures proposed for the nonradical peroxo niobium species are shown in Fig. 6.

Generation of HO• and HO₂ in Nb-catalyzed oxidation is evident, since unproductive decomposition of hydrogen peroxide always occurs along with organic substrate oxidation (H₂O₂ utilization efficiency in alkene epoxidation is typically in the range of 50–65%) [26,29]. The formation of NbO• and NbO₂ species upon decomposition of H₂O₂ over Nb silicates may occur via mechanisms similar to those proposed for Ti silicates [10,67]. Generation of the superoxo niobium species Nb^VO₂⁻ on the surface of Nb catalysts was previously confirmed by ESR [38,39]. A shoulder at 320 nm in DR UV-vis spectra of H₂O₂-treated amorphous Nb₂O₅ has been assigned to such species [39]. More recently, a similar absorption band (310 nm) was found for H₂O₂-treated Nb-Beta and assigned to an unusual superoxide designated as Nb^{IV}-(O₂)⁻ or Nb^{IV}-(O₂)⁻ [40]. On the basis of results of in situ UV-vis spectro-

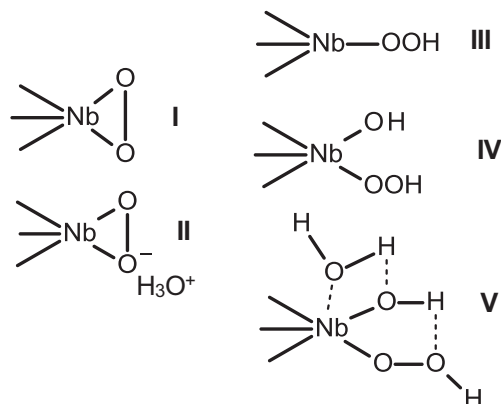
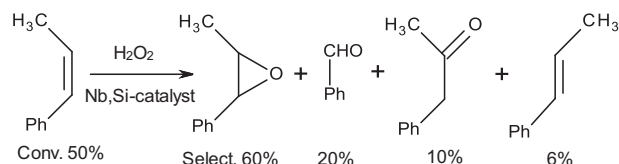


Fig. 6. Structures of peroxo and hydroperoxo niobium species proposed in the literature: **I** [65], **II** [66], **III** [32], **IV** [14,32], and **V** [31].

scopic studies, it has been inferred to be the active epoxidizing species. Although the ability of mesoporous niobium silicates to decompose H₂O₂ is lower than that of their titanium counterparts (Fig. 4), it is not negligible, and one might expect a contribution of radical species to the oxidation process. On the other hand, one of the main arguments against a radical mechanism of epoxidation over Nb is the high heterolytic pathway selectivity in the oxidation of cyclohexene. This olefin is a well-known test substrate for discrimination between homolytic and heterolytic oxidation processes, since it possesses highly reactive C–H bonds in the allylic position, which react easily with radical species, resulting in allylic oxidation products [68]. For niobium silicates, total heterolytic pathway selectivity in cyclohexene oxidation typically varies in the range 70–99%, depending on the degree of Nb site isolation and the reaction conditions [13,15,23,24,28–30]. In general, it is superior to that of mesoporous titanium silicates, for which allylic oxidation products are present in pronounced amounts when H₂O₂ is employed as oxidant [11,12]. For example, SiO₂-grafted Nb(V) catalysts (Nb–SiO₂) demonstrated 88–90% selectivity toward cyclohexene oxide and *trans*-diol at ca. 100% total yield, while Ti–SiO₂ prepared by the same methods gave only 65–67% of these products at 69–93% total yield [30]. The data presented in Table 3 also demonstrate that Nb silicates prepared by EISA (both **A** and **B**) reveal higher heterolytic pathway selectivity than titanium silicate **A-Ti** (85–88% vs 70% at 30 °C). A similar trend was established for oxidation of limonene, another substrate with reactive allylic hydrogen atoms [21].

Finally, stereospecificity in epoxidation of *cis*-alkenes is another strong argument in favor of a nonradical epoxidizing species and heterolytic concerted epoxidation mechanism that involves no radical or ionic intermediate capable of rotation over C–C bonds (such a species would lead to at least partial loss of the initial configuration and formation of *trans*-epoxide). Indeed, epoxidation of methyl oleate (methyl *cis*-9-octadecenoate) in the presence of mesoporous Nb catalysts produced solely methyl *cis*-9,10-epoxyoctadecanoate [17,22]. In contrast, some amounts of the corresponding *trans*-isomer formed in the presence of mesoporous titanium-silicates under similar reaction conditions [69]. The oxidation of *cis*-β-methylstyrene over Nb silicates (both catalysts **A** and **B**) also proceeded with retention of the *cis*-configuration, producing *cis*-epoxide as the main oxidation product (Scheme 1). The amount of the corresponding *trans*-epoxide was less than 1%.



Scheme 1. Oxidation of *cis*-β-methylstyrene over mesoporous niobium silicate. Reaction conditions: alkene 0.1 M, H₂O₂ 0.1 M, catalyst 0.003 mmol Nb, MeCN 1 mL, 50 °C, 6 h.

We also attempted to check stereospecificity in the oxidation of *cis*-stilbene, an olefin substrate highly prone to the formation of *trans*-epoxide in case of radical epoxidizing species [70]. *Cis*-epoxide was found in the reaction mixture in a low yield, while *trans*-epoxide was not present at all. However, the main oxidation product was benzaldehyde; therefore, this test was less unambiguous than that with *cis*- β -methylstyrene, where *cis*-epoxide was the principal reaction product. *Trans*-stilbene was ca. fivefold less reactive than *cis*-stilbene, indicating that steric factors have a strong impact on the oxidation process over the Nb catalysts.

The distinctive features of epoxidation over mesoporous niobium-silicates, such as minor or negligible amount of allylic oxidation products and the retention of configuration of *cis*-olefins, are only consistent with a heterolytic mechanism. Therefore, we can rule out any radical species as the species responsible for the selective formation of epoxides and suggest a concerted transfer of oxygen atoms from a peroxo niobium species to a nucleophilic C=C bond.

3.8. Active niobium species: Hydroperoxo vs. peroxo

The next question that arises is whether the active epoxidizing species is peroxo Nb(η^2 -O₂) or hydroperoxo NbOOH (the latter may also include hydroxyl and water molecules, as shown in Fig. 6). By analogy with titanium, the formation of peroxo complexes is associated with the reaction of the Nb=O group with H₂O₂, while the formation of hydroperoxo species can be envisaged in two steps [32]:



Strukul and co-workers suggested that one Nb(V) center can bear two OH groups, one of which is replaced with a hydroperoxo group upon interaction with H₂O₂, leading to Nb(OH)OOH (structure IV in Fig. 6) [14]:

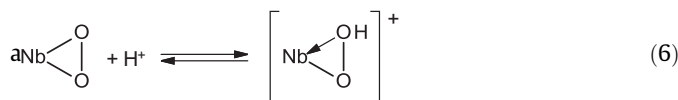


More recently, Notestein and co-workers also assumed that individual Nb sites may hydrolyze under reaction conditions to form two NbOH bonds with both NbOH on the same Nb atom [31]. Then they suggested that one of the hydroxyls takes the role of assisting (similarly to the role of alcohol in Ti-catalyzed oxidation [10]) in the rate-limiting oxygen transfer step, while the other forms the bound hydroperoxo species (species V in Fig. 6). In this case, the water molecule remains coordinated on the Nb(OH)OOH species:



As implied by vibrational spectroscopic [25,71,72] and computational [53,73,74] techniques, both Nb=O and Nb-OH groups can be present on the surfaces of niobium silicates. The ratio between them, as well as the degree of isolation/polymerization, may depend on the preparation methodology as well as on the hydration or dehydration state of the surface. Tielens et al. revealed that the most favorable Nb(V) structure in zeolite Nb- β is one having a Nb(V)OH group linked to the zeolitic walls by four Nb-OSi bonds [53]. The Nb(V)=O site is less stable but becomes similar in stability when hydrated. Later on, it was shown using periodic density functional theory for a systematic investigation of a series of model zeolites that the M=O group is more stabilized for M = vanadium, while M-OH is more favorable for M = niobium or tantalum [73]. Therefore, generation of both peroxo and hydroperoxo species might be expected through interaction of the surface Nb=O and

NbOH species with H₂O₂ via Eqs. (1)–(5). Peroxo and hydroperoxo species may be present at an equilibrium (counteranion is not shown) that would shift right or left, depending on the surface and medium acidity:



In 1991, Clerici first suggested that hydroperoxo Ti-OOH rather than peroxo Ti(η^2 -O₂) is responsible for the catalytic activity of TS-1 [75]. One of the main indications in favor of Ti-OOH was a rate-inhibiting effect of basic compounds on the catalytic activity and, in opposition, a rate-accelerating effect of acids [75,76]. This suggestion was further supported by chemical, spectroscopic, and computational studies, and Ti-OOH species became a widely accepted concept over the years, extended later to other Ti-containing molecular sieves (for recent reviews, see Refs. [10,11]). This prompted us to investigate effects of acids and bases on the catalytic performance of mesoporous niobium silicates. The results are provided in Table 4, where we also include data acquired for the mesoporous catalyst A-Ti. Addition of sodium acetate in an amount close to the amount of Nb sites retarded the rate of CyO oxidation substantially (TOF 0.18 vs. 0.39 min⁻¹), which strongly supports the hypothesis about hydroperoxo niobium(V) as the real epoxidizing species in the system. Indeed, according to Eq. (6), bases are expected to transform NbOOH to Nb(η^2 -O₂). A similar effect was found for the mesoporous Ti catalyst (TOF 0.22 vs. 0.35 min⁻¹). In contrast to alkene epoxidation over TS-1 [76], the influence of acid on the CyO oxidation rate turned out to be minor for mesoporous Nb and Ti silicates (see Table 4). This may be rationalized if we remember that TS-1 is hydrophobic and contains mostly tetrahedrally coordinated Ti (OSi)₄ sites, which are partially hydrolyzed in the presence of water to produce highly reactive Ti-OH species, whereas mesoporous Nb and Ti silicates already have a significant number of M-OH (M = Nb or Ti) groups on their surface.

The peroxo species formed upon interaction of the Nb catalysts with H₂O₂ was probed by a DR UV-vis spectroscopic technique. Fig. 7 shows changes in the DR UV-vis spectrum of catalyst B after treatment with aqueous H₂O₂. The appearance of the new absorption band with a maximum at 307 nm (curve B) responsible for the pale yellow color of the H₂O₂-treated sample is associated with reaction of the Nb(V) center with hydrogen peroxide.

Table 4

Effects of acid and base additives on CyO and MNQ oxidation with H₂O₂ over Nb and Ti silicates.

Catalyst	Substrate	Additive	TOF, min ^{-1a}
A	CyO	–	0.39
		NaOAc	0.18 ^b
		HClO ₄	0.38
A-Ti	CyO	–	0.35
		NaOAc	0.22
		HClO ₄	0.37
A	MNQ	–	0.04
		NaOAc	0.15
		HClO ₄	0.04
A-Ti	MNQ	–	No reaction

Notes: Reaction conditions: substrate 0.1 mmol, catalyst 0.003 mmol Nb or Ti, additive 0.003 mmol (if any), H₂O₂ 0.1 mmol and 50 °C (CyO) or H₂O₂ 0.4 mmol and 70 °C (MNQ), MeCN 1 mL.

^a TOF = (moles of substrate consumed)/(moles of metal × time), determined by GC from initial rates of substrate consumption.

^b Similar result with 2 equiv. of NaOAc.

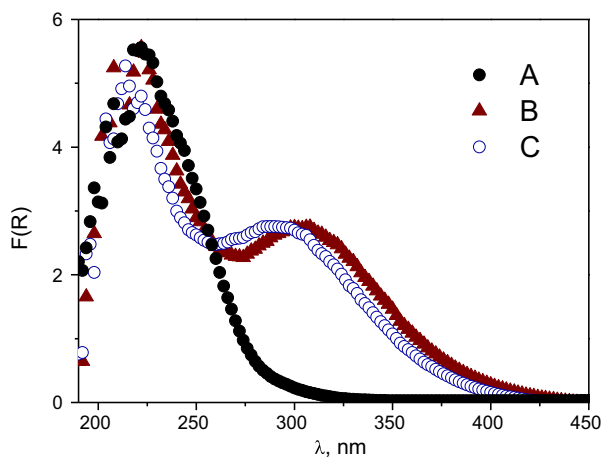


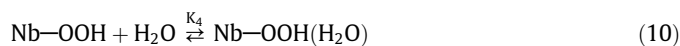
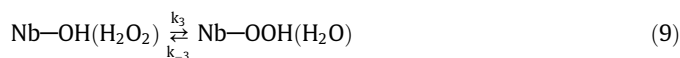
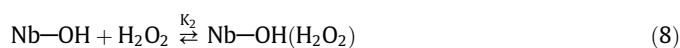
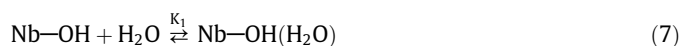
Fig. 7. DR UV-vis spectra of catalyst **B** before (A) and after treatment with $\text{H}_2\text{O}_2/\text{H}_2\text{O}$ (B) and $\text{H}_2\text{O}_2/\text{H}_2\text{O}/\text{NaOAc}$ (C). Treatment conditions: catalyst 0.57 g (0.11 mmol Nb), MeCN 6 mL, 30% H_2O_2 2 mL, H_2O 5 mL, NaOAc (if any) 0.16 mmol, 15 min, room temperature.

Recently, DR UV-vis absorption features at 320 [39] and 335 [40] nm were observed for amorphous niobia and zeolite Nb-Beta, respectively, after interaction with H_2O_2 and, as was already mentioned above, these bands were assigned to superoxo niobium species, referring to TS-1. However, it is widely accepted that the DR UV-vis absorption at 350–400 nm (specifically, 385 nm for TS-1), which appears after interaction of titanium silicates with H_2O_2 in addition to the parent $\text{Ti}^{4+}\text{O}^{2-} \rightarrow \text{Ti}^{3+}\text{O}^-$ ligand-to-metal charge transfer (LMCT) band at 208–250 nm, is ascribed to LMCT from a O–O moiety to the Ti center and therefore belongs to (hydro)peroxo rather than superoxo titanium species [10,77–81]. A yellow or light yellow color is characteristic of several Nb(V) peroxo complexes, for which bidentate (η^2) coordination of the peroxo ligand has been proved by single crystal X-ray analysis [82–84]. Generally, niobium peroxo complexes with a peroxo-to-Nb molar ratio of 1:1 reveal UV-vis absorption features at 255–280 nm [85–88], while complexes with Nb bearing more than one peroxo ligand may absorb also at 325–380 nm [84–86,89]. Importantly, after treatment of the Nb peroxo derivative with aqueous NaOAc, the DR UV-vis absorption feature shifted from 307 to 293 nm (curve C in Fig. 7). A blue shift was previously observed in the DR UV-vis spectrum of H_2O_2 -treated TS-1 after subsequent dosage with an NH_3 or NaOH aqueous solution, and it was attributed to the transformation of an open, end-on hydroperoxo ($\equiv\text{SiO}_3(\text{H}_2\text{O})_2\text{TiOOH}$) species into a more stable side-on peroxo complex [90]. Concerning niobium peroxo species, it was mentioned in the literature that their color changed from yellow at pH ~ 1 to pale yellow at pH ~ 3 [87]. On the other hand, a pronounced bathochromic shift was observed in the UV-vis spectra of the H_2O_2 -Nb $_2\text{O}_5$ - H_2SO_4 system as the sulfuric acid concentration was increased [85]. All these facts collectively have led us to the conclusion that the absorption feature at 307 nm arising after interaction of catalyst **B** with aqueous H_2O_2 can be assigned to a protonated peroxo Nb(V) species (i.e., the hydroperoxo species NbOOH), which undergoes transformation to the peroxo species Nb(η^2 -O $_2$) after deprotonation under the action of base. The negative effect of base on the catalytic activity of niobium silicates in epoxidation of electron-rich alkenes (Table 4) allowed us to suggest that NbOOH rather than Nb(η^2 -O $_2$) is the true epoxidizing species that operates with H_2O_2 . Whether the hydroperoxo moiety has η^1 or η^2 coordination is still an open question. It should be noted, however, that the debate about the coordination mode of the hydroperoxo group in titanium silicate catalysts is still ongoing

(for recent reviews, see Refs. [10,11]). Interestingly, DFT calculations recently performed using model compounds, early-transition-metal-substituted Keggin polyoxometalates $[\text{PTM}(\text{O}_2)(\text{H})\text{W}_{11}\text{O}_{39}]^{n-}$ (TM = Ti(IV), V(V), Zr(IV), Nb(V), Mo(VI), W(VI), and Re(VII)), showed that, similarly to Ti(IV), the oxygen transfer energy barrier is ca. 9 kcal·mol $^{-1}$ lower for NbOOH than for Nb(O $_2$) [35].

3.9. Rate law and mechanism of CyO epoxidation over niobium silicates

The kinetic regularities established for CyO oxidation over the niobium silicates (saturation kinetics and first-order rate dependence on catalyst were shown in Fig. 2) are similar to those observed earlier for alkene epoxidation with H_2O_2 over TS-1 [10] and grafted Ta-SBA-15 [91], heterogeneous catalysts known for their high heterolytic pathway selectivity. Hence, we may suppose that an Eley–Rideal-type mechanism can be employed for description of Nb-catalyzed CyO epoxidation with H_2O_2 . Such mechanism may involve the following steps: adsorption of water and H_2O_2 on undercoordinated Nb centers (the presence of LAS has been confirmed by FTIR spectroscopy with adsorption of CO and Py), H_2O_2 activation through reversible interaction with NbOH to give NbOOH followed by electrophilic oxygen transfer from NbOOH to C=C bond, producing epoxide and regenerating the initial state of the catalyst. The equilibrium of adsorption/desorption of water on/from NbOOH site should also be taken into account. We can neglect the step of adsorption of epoxide product on Nb centers because no effect of the epoxide on the reaction rate was established experimentally:

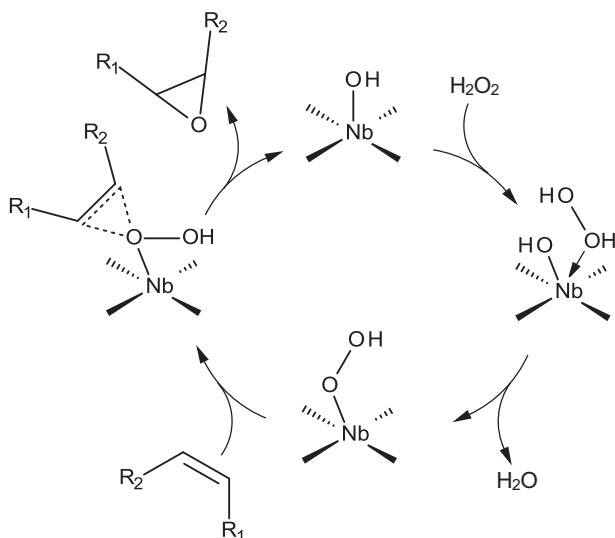


By applying a steady-state approximation to the concentration of the active species NbOOH, the rate law represented by Eq. S1 (see the SI for details) was derived. After fitting of the experimental data with this rate law, parameters k_{-3} and K_4 were found to be close to zero (Table S1), indicating that the formation of NbOOH from NbOH and H_2O_2 is almost irreversible and is accompanied by instant release of water molecules. Under this assumption, a simplified rate law can be derived (see SI for details):

$$W_0 = \frac{K_2 k_3 [\text{H}_2\text{O}_2] n(\text{Nb})_0}{V \left(1 + K_1 [\text{H}_2\text{O}] + \frac{K_2 k_3 [\text{H}_2\text{O}_2]}{k_5 [\text{CyO}]} \right)} \quad (12)$$

where $n(\text{Nb})_0$ is the total number of accessible Nb sites and V is the volume of the reaction mixture.

Eq. (12) describes the observed kinetic regularities well, including the dependence of the initial reaction rate on the concentration of water (fitting of the experimental points is shown in Fig. 2). However, we should also mention here that a rate law similar to that depicted by Eq. (12) might be obtained under the assumption that Nb(OH) $_2$ reacted with H_2O_2 via Eq. (4). Therefore, our kinetic results are, in principle, consistent with both NbOOH and Nb(OH) $_2$ OOH active species.



Scheme 2. Proposed catalytic cycle for alkene epoxidation with H_2O_2 over Nb silicates.

The catalytic cycle proposed for epoxidation of electron-rich alkenes is shown in Scheme 2. It is fully consistent with all the results acquired in this work, including the kinetic and spectroscopic data, the rate retarding effect of bases, high heterolytic pathway selectivity in the epoxidation of cyclohexene, and stereospecificity of the epoxidation of *cis*- β -methylstyrene.

A comparative FTIR spectroscopic study using probe molecules (Py and CO) performed on niobium and titanium silicates prepared by the same EISA technique showed that the strength of LAS is somewhat higher for Nb catalysts (see Table 2 and discussion in Section 3.2), which may account for their superior heterolytic

selectivity in H_2O_2 -based oxidation of electron-rich alkenes. This agrees with the results recently reported by Notestein and co-workers, who revealed that direct cyclohexene epoxidation rates correlate well with an ionic bond character of the supported oxide [30]. However, higher heterolytic oxidation selectivity could also be due to a higher energy barrier to homolytic O–O bond breaking in the hydroperoxo intermediate, similarly to homogeneous Ti-containing polyoxometalates [35].

3.10. Kinetics of MNQ epoxidation

The reaction rates of MNQ oxidation over catalysts **A** and **B** turned out to be at least two orders of magnitude lower than the rates of CyO epoxidation. Fig. 8 shows dependences of the initial rates of MNQ consumption over catalyst **A** on concentrations of all reagents. Similar dependences were found for catalyst **B**. The reaction was found to be first-order in catalyst (Fig. 8a) and H_2O_2 (Fig. 8c), zero-order in MNQ (Fig. 8b), and nearly zero-order in H_2O (Fig. 8d). Therefore, the kinetic regularities found for MNQ differ significantly from those established for CyO (Fig. 2).

Similar epoxidation rates were found for MNQ and another quinone, 2,3,5-trimethyl-1,4-benzoquinone. Coupled with reaction order zero in MNQ, this fact indicates that the quinone substrate does not participate in the rate-limiting step of the epoxidation process. Apparent activation energies determined from Arrhenius dependences (Fig. 9) are 13.9 and 12.3 kcal/mol for catalysts **A** and **B**, respectively, which is somewhat high compared with E_a of CyO epoxidation (see Fig. 3). However, their values still remain lower than the activation energies of H_2O_2 decomposition, which were 20.5 and 16.6 kcal/mol for catalysts **A** and **B**, respectively (see Fig. 5).

As one can see from the plots in Fig. 9, the rate of MNQ epoxidation was a little higher for catalyst **A** than for catalyst **B** in the range of temperatures used, while an opposite trend was observed

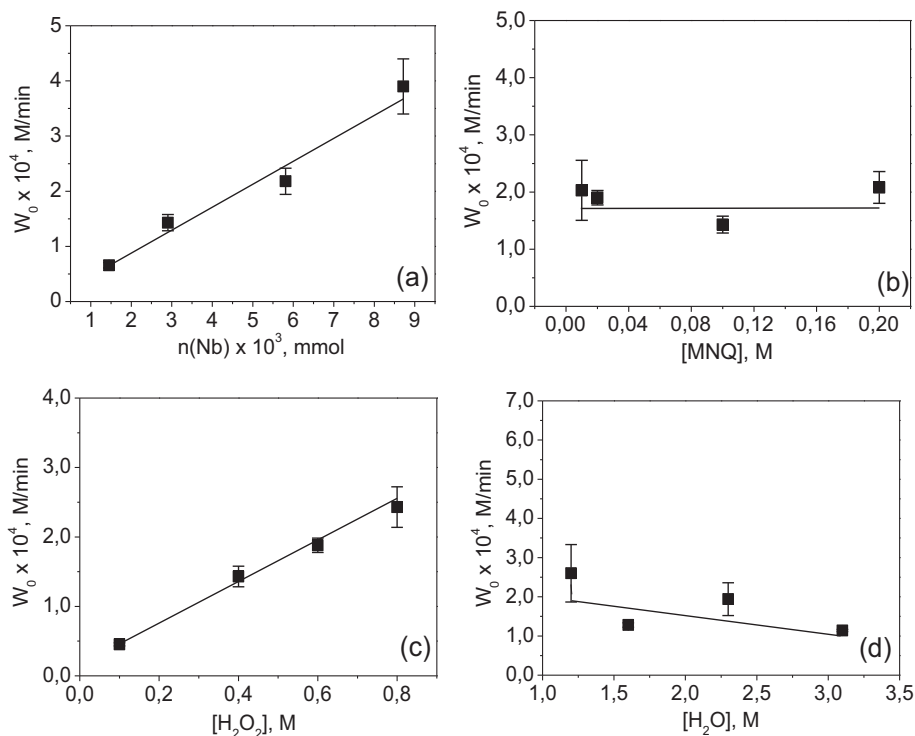


Fig. 8. Plots of the initial rate of MNQ oxidation (MeCN, 70 °C) over catalyst **A** versus concentration of catalyst (a), substrate (b), oxidant (c), and water (d). For other reaction conditions, see Section 2.3.

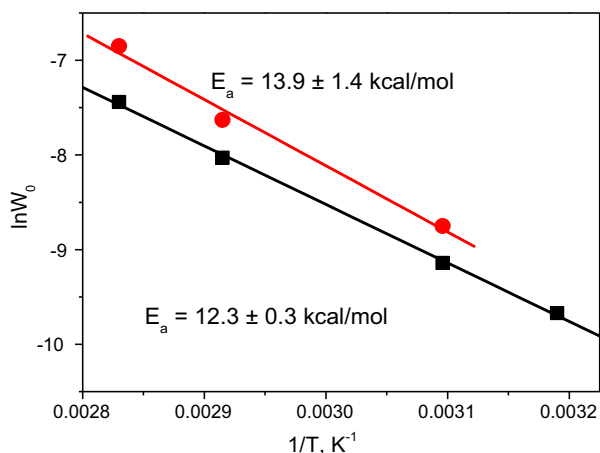


Fig. 9. Arrhenius plots for MNQ oxidation over catalysts **A** (●) and **B** (■). Reaction conditions: MNQ 0.1 M, H₂O₂ 0.4 M, catalyst 0.003 mmol Nb, MeCN 1 mL, 40–80 °C.

in the epoxidation of CyO (Fig. 3). Possible reasons for this will be addressed in the following sections.

3.11. Active species responsible for MNQ epoxidation

As already mentioned, the rate of MNQ epoxidation over Nb silicates was not affected by light, molecular oxygen, or addition of radical chain scavengers. We should also recall here that mesoporous titanium silicates are practically inactive in epoxidation of α,β -unsaturated carbonyl compounds. Accordingly, epoxyquinones were minor byproducts in the oxidation of alkylphenols to benzoquinones over Ti catalysts [92], but their yield greatly increased under the same conditions if Nb -catalysts were employed [29]. Indeed, no reaction occurred when MNQ was subjected to oxidation using H₂O₂ and catalyst **A-Ti** (Table 3). Therefore, we may conclude that there is no correlation between the catalyst's ability to decompose hydrogen peroxide (Fig. 4) and epoxidize MNQ. All these facts collectively imply that a nonradical oxidation mechanism operates in the Nb-catalyzed oxidation of α,β -unsaturated carbonyl compounds.

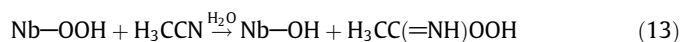
It is remarkable that the effect of base on the epoxidation of MNQ is opposite to the effect found for CyO epoxidation (see Table 4). The rate of MNQ oxidation increased approximately four

times upon addition of NaOAc. This fact has prompted us to the thought that probably we deal with the so-called Payne oxidation, which normally requires basic conditions [93]. In this case, the epoxidation rate is essentially independent of olefin structure because the slow step in the process is oxidation of the solvent, MeCN, to give a peroxycarboximidic acid intermediate, H₃CC(=NH)OOH, which is the real epoxidizing species that reacts with electron-deficient C=C bonds. Indeed, conversion of MNQ became negligible (<5%) when acetonitrile was replaced with another solvent, ethyl acetate. Finally, acetamide (the product derived from peroxyimidic acid) was found in the reaction mixture in an amount comparable to that of epoxide formed from MNQ. No acetamide was present when the oxidizing substrate was electron-rich alkene (CyO or limonene) or titanium silicate **A-Ti** was used as the catalyst. Earlier, on the basis of specific tests and spectroscopic analyses, Guidotti et al. excluded the formation of peroxyimidic acid during alkene epoxidation with H₂O₂ over mesoporous titanium silicates [94]. On the other hand, the same team suggested that Payne-type oxidation may contribute to the epoxidation of methyl oleate due to the presence of residual amounts of basic transesterification catalysts in the commercial samples of this substrate [69].

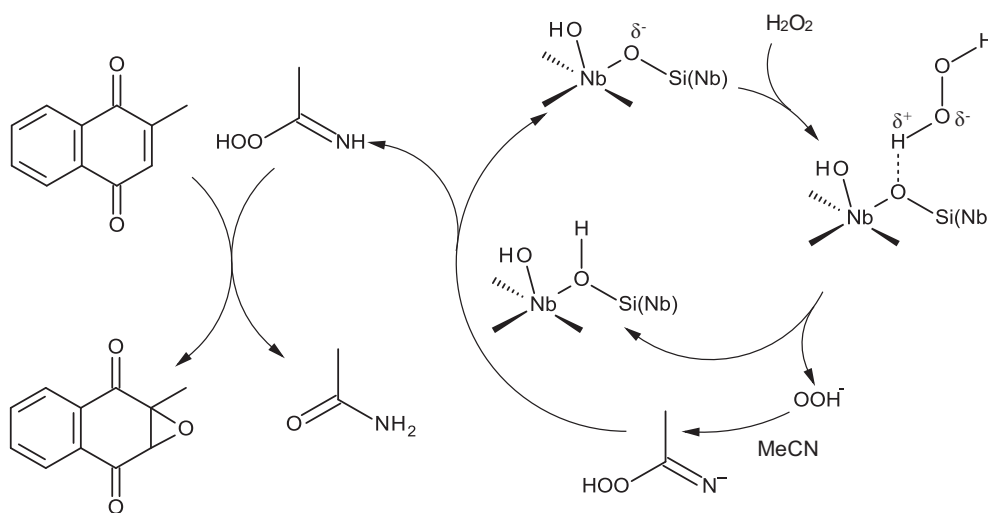
Therefore, we may conclude that the ability to epoxidize electron-deficient double bonds in α,β -unsaturated carbonyl compounds, characteristic of mesoporous Nb silicates, is in fact related to their ability to oxidize MeCN and accomplish Payne-type oxidation.

3.12. Proposed mechanism for MNQ epoxidation

Two alternative mechanisms, both involving peroxycarboximidic acid and consistent with the observed kinetic regularities, can be envisaged for MNQ epoxidation over niobium silicate catalysts. The first one may involve steps leading to the formation of hydroperoxo species NbOOH (Eqs. (7)–(10)), followed by rate-limiting oxidation of MeCN with this species to produce peroxyimidic acid and oxygen transfer from the latter to C=C bonds, giving epoxy derivatives (MNQO) and acetamide:

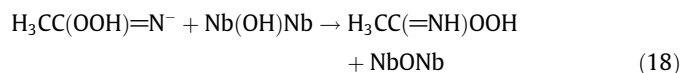
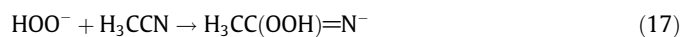
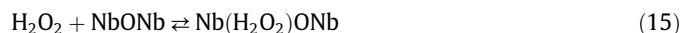


An alternative mechanism may involve hydrogen peroxide activation through adsorption and dissociation on a basic site, which is, most likely, NbOSi or NbONb (the second option is shown



Scheme 3. Tentative mechanism for epoxidation of α,β -unsaturated carbonyl compounds with H₂O₂ over Nb catalysts.

below), slow oxidation of MeCN with HOO^- to afford an anionic intermediate that takes protons from the catalyst, thereby regenerating its initial form and producing peroxyimidic acid, followed by oxygen transfer from the peroxy acid to C=C bond (Eq. (14)):



Previously, participation of peroxycarboximidic acid in alkene epoxidation with H_2O_2 in the presence of nitriles was implied for the well-known hydrotalcite basic catalysts [95–97], and a similar mechanism engaging hydrogen peroxide activation on basic sites was proposed [97]. Although basic sites in niobium silicates are weaker than in layered double hydroxides (PA 780 vs 850–920 kJ/mol [98]), we may tentatively assume their participation in nucleophilic activation of hydrogen peroxide. In turn, the inertness of titanium silicates in epoxidation of α,β -unsaturated carbonyl compounds can be explained by the lack of basic sites in these catalysts. Recent DFT calculations revealed that the most basic site in Nb- β is the bridging oxygen of the Nb–O–Si site [53]. Our estimates by FTIR using adsorbed CDCl_3 showed a similar strength of basic sites in catalysts **A** and **B** (see Table 2). On the other hand, somewhat higher activity of catalyst **A** in MNQ epoxidation (Fig. 9) correlates with a higher concentration of basic sites in this catalyst, which in turn, correlates with the number of Nb–O–Nb connectivities.

Scheme 3 presents a tentative mechanism for the selective epoxidation of α,β -unsaturated carbonyl compounds (e.g., MNQ) catalyzed by niobium silicates. This mechanism is compatible with all the data obtained in this work (kinetics, products, additives, and solvent effects) and is also supported by the detection of basic sites in the niobium catalysts.

4. Conclusions

The results acquired in this work using kinetic, product, and spectroscopic tools indicated two different mechanisms for H_2O_2 -based epoxidation of electron-rich and electron-deficient C=C bonds over mesoporous niobium silicates. Epoxidation of electron-rich alkenes involves adsorption of H_2O_2 on coordinatively unsaturated Nb(V) sites, interaction with H_2O_2 to give a hydroperoxo species NbOOH and water, followed by a concerted electrophilic oxygen transfer from NbOOH to C=C bonds, producing epoxides and regenerating the initial state of the catalyst. This mechanism is compatible with all the data gained in this study and reported in the literature for mesoporous Nb silicates, specifically the rate law established for CyO epoxidation (first order in catalyst and fractional, <1, orders in alkene and oxidant), rate-retarding effect of base, stereospecificity in the epoxidation of *cis*-alkenes, and high heterolytic pathway selectivity in oxidation of alkenes with highly reactive allylic hydrogen atoms, such as cyclohexene and limonene. The hydroperoxo niobium species is manifested in DRS UV–vis by an absorption band at 307 nm, which reveals a blue shift after treatment with an aqueous solution of NaOAc.

Several lines of evidence, including the established rate law (zero order in substrate and first order in catalyst and H_2O_2), the rate-accelerating effect of base, the formation of acetamide in the amount close to that of epoxide, the lack of reaction in ethyl acetate, and the detection of weak basic sites on the surface of niobium silicates by IR spectroscopy using CDCl_3 as a probe molecule, all

indicate that epoxidation of α,β -unsaturated carbonyl compounds proceeds through the so-called Payne oxidation, which involves rate-limiting oxidation of the solvent molecule (MeCN) by a peroxo niobium species or, more likely, HOO^- formed upon interaction of H_2O_2 with a basic site (Nb–O–Nb or Nb–O–Si), leading to the formation of peroxycarboximidic acid, $\text{H}_3\text{CC}(\text{=NH})\text{OOH}$, which reacts with electron-deficient C=C bonds, producing epoxy derivatives and acetamide. A comparative FTIR spectroscopic study using various probe molecules (Py, CO, and CDCl_3) performed on the niobium and titanium silicates prepared by the same EISA technique revealed two main differences: (1) the amount and strength of LAS and BAS is somewhat higher in Nb silicates than in their Ti counterparts and (2) Nb silicates possess weak basic sites while Ti silicates do not; the number of basic sites is larger for catalysts with di(oligo)meric Nb sites. The higher strength of LAS may account for the superior heterolytic pathway selectivity in H_2O_2 -based oxidation of alkenes over mesoporous niobium silicates, while the higher strength of BAS may be the reason for various rearrangements observed in the oxidation of acid-sensitive substrates. The presence of weak basic sites may explain why mesoporous niobium silicate catalysts are able to epoxidize α,β -unsaturated carbonyl compounds while their Ti analogs are not. The results obtained in this work allowed us to suggest that the presence of both Lewis acidic and basic sites ensures the ability of mesoporous niobium silicate to activate hydrogen peroxide by two different modes, leading to electrophilic (NbOOH) and nucleophilic (HOO^-) active species, which, in turn, accomplish epoxidation of electron-rich and electron-deficient C=C bonds, respectively. Further spectroscopic, computational, and kinetic studies on model Nb-containing systems are in progress in our group to gain further insight into the mechanisms of H_2O_2 activation and Nb-catalyzed oxidations.

Acknowledgments

The authors thank M.G. Clerici for fruitful discussions. The help of Dr. S.A. Yashnik in DRS UV–vis measurements is greatly appreciated. This work was carried out in the framework of budget project 0303-2016-0005 for the Boreskov Institute of Catalysis and partially supported by the Russian Foundation for Basic Research (Grant 16-03-00827).

Appendix A. Supplementary material

Supplementary data associated with this article can be found, in the online version, at <https://doi.org/10.1016/j.jcat.2017.09.011>.

References

- [1] R.A. Sheldon, M.C.A. van Vliet, in: *Fine Chemicals through Heterogeneous Catalysis*, Wiley-VCH, Weinheim, 2001, p. 473.
- [2] F. Cavani, J.H. Teles, Sustainability in catalytic oxidation: an alternative approach or a structural evolution?, *ChemSusChem* 2 (2009) 508–534.
- [3] G. Strukul (Ed.), *Catalytic Oxidations with Hydrogen Peroxide as Oxidant*, Kluwer Academic, Dordrecht, 1992.
- [4] B.S. Lane, K. Burgess, Metal-catalyzed epoxidations of alkenes with hydrogen peroxide, *Chem. Rev.* 103 (2003) 2457–2474.
- [5] G. Grigoropoulou, J.H. Clark, J.A. Elings, Recent developments on the epoxidation of alkenes using hydrogen peroxide as an oxidant, *Green Chem.* 5 (2003) 1–7.
- [6] R. Sheldon, I.W.C.E. Arends, U. Hanefeld, *Green Chemistry and Catalysis*, Wiley-VCH, Weinheim, 2007.
- [7] M.G. Clerici, O.A. Kholdeeva (Eds.), *Liquid Phase Oxidation via Heterogeneous Catalysis: Organic Synthesis and Industrial Applications*, Wiley, Hoboken, New Jersey, 2013.
- [8] B. Notari, in: D.D. Eley, W.O. Haag, B.C. Gates (Eds.), *Adv. Catal.* 41 (1996) 253–334.
- [9] C. Perego, A. Carati, P. Ingallina, M.A. Mantegazza, G. Bellussi, Production of titanium containing molecular sieves and their application in catalysis, *Appl. Catal. A: Gen.* 221 (2001) 63–72.

- [10] For recent review see: M.G. Clerici, M.E. Domine, in: *Liquid Phase Oxidation via Heterogeneous Catalysis: Organic Synthesis and Industrial Applications*, Wiley, Hoboken, New Jersey, 2013, pp. 21–93.
- [11] O.A. Kholdeeva, in: *Liquid Phase Oxidation via Heterogeneous Catalysis: Organic Synthesis and Industrial Applications*, Wiley, Hoboken, New Jersey, 2013, pp. 127–219.
- [12] O.A. Kholdeeva, Recent developments in liquid-phase selective oxidation using environmentally benign oxidants and mesoporous metal silicates, *Catal. Sci. Technol.* 4 (2014) 1869–1889.
- [13] I. Nowak, B. Kilos, M. Ziolk, A. Lewandowska, Epoxidation of cyclohexene on Nb-containing meso- and macroporous materials, *Catal. Today* 78 (2003) 487–498.
- [14] F. Somma, P. Canton, G. Strukul, Effect of the matrix in niobium-based aerogel catalysts for the selective oxidation of olefins with hydrogen peroxide, *J. Catal.* 229 (2005) 490–498.
- [15] I. Nowak, M. Ziolk, Effect of texture and structure on the catalytic activity of mesoporous niobosilicates for the oxidation of cyclohexene, *Micropor. Mesopor. Mater.* 78 (2005) 281–288.
- [16] F. Somma, G. Strukul, Niobium containing micro-, meso- and macroporous silica materials as catalysts for the epoxidation of olefins with hydrogen peroxide, *Catal. Lett.* 107 (2006) 73–81.
- [17] A. Feliczak, K. Walczak, A. Wawrynczak, I. Nowak, The use of mesoporous molecular sieves containing niobium for the synthesis of vegetable oil-based products, *Catal. Today* 140 (2009) 23–29.
- [18] M. Selvaraj, S. Kawi, D.W. Park, C.S. Ha, A merit synthesis of well-ordered two-dimensional mesoporous niobium silicate materials with enhanced hydrothermal stability and catalytic activity, *J. Phys. Chem. C* 113 (2009) 7743–7749.
- [19] A. Feliczak-Guzik, I. Nowak, Mesoporous niobosilicates serving as catalysts for synthesis of fragrances, *Catal. Today* 142 (2009) 288–292.
- [20] I. Nowak, Frontiers in mesoporous molecular sieves containing niobium: from model materials to catalysts, *Catal. Today* 192 (2012) 80–88.
- [21] C. Gallo, R. Tiozzo, F. Psaro, M. Carniato, Guidotti, Niobium metallocenes deposited onto mesoporous silica via dry impregnation as catalysts for selective epoxidation of alkenes, *J. Catal.* 298 (2013) 77–83.
- [22] C. Tiozzo, C. Bisio, F. Carniato, L. Marchese, A. Gallo, N. Ravasio, R. Psaro, M. Guidotti, Epoxidation with hydrogen peroxide of unsaturated fatty acid methyl esters over Nb(V)-silica catalysts, *Eur. J. Lipid Sci. Technol.* 115 (2013) 86–93.
- [23] C. Tiozzo, C. Bisio, F. Carniato, A. Gallo, S.L. Scott, R. Psaro, M. Guidotti, Niobium-silica catalysts for the selective epoxidation of cyclic alkenes: the generation of the active site by grafting niobocene dichloride, *Phys. Chem. Chem. Phys.* 15 (2013) 13354–13362.
- [24] C. Tiozzo, C. Bisio, F. Carniato, M. Guidotti, Grafted non-ordered niobium-silica materials: versatile catalysts for the selective epoxidation of various unsaturated fine chemicals, *Catal. Today* 235 (2014) 49–57.
- [25] R. Turco, A. Aronne, P. Carniti, A. Gervasini, L. Minieri, P. Pernice, R. Tesser, R. Vitiello, M. Di Serio, Influence of preparation methods and structure of niobium oxide-based catalysts in the epoxidation reaction, *Catal. Today* 254 (2015) 99–103.
- [26] C. Tiozzo, C. Palumbo, R. Psaro, C. Bisio, F. Carniato, A. Gervasini, P. Carniti, M. Guidotti, The stability of niobium-silica catalysts in repeated liquid-phase epoxidation tests: a comparative evaluation of in-framework and grafted mixed oxides, *Inorg. Chim. Acta* 431 (2015) 190–196.
- [27] A. Ramanathan, R. Mageshwar, B. Subramanian, Facile styrene Epoxidation with H₂O₂ over novel niobium containing cage type mesoporous silicate, Nb-KIT-5, *Top. Catal.* 58 (2015) 314–324.
- [28] A. Ramanathan, H. Zhu, R. Mageshwar, P.S. Thapa, B. Subramanian, Comparative study of Nb-incorporated cubic mesoporous silicates as epoxidation catalysts, *Ind. Eng. Chem. Res.* 54 (2015) 4236–4242.
- [29] I.D. Ivanchikova, N.V. Maksimchuk, I.Y. Skobelev, V.V. Kaichev, O.A. Kholdeeva, Mesoporous niobium-silicates prepared by evaporation-induced self-assembly as catalysts for selective oxidations with aqueous H₂O₂, *J. Catal.* 332 (2015) 138–148.
- [30] N.E. Thornburg, A.B. Thompson, J.M. Notestein, Periodic trends in highly dispersed groups IV and V supported metal oxide catalysts for alkene epoxidation with H₂O₂, *ACS Catal.* 5 (2015) 5077–5088.
- [31] N.E. Thornburg, S.L. Nauert, A.B. Thompson, J.M. Notestein, Synthesis-structure-function relationships of silica-supported niobium(V) catalysts for alkene epoxidation with H₂O₂, *ACS Catal.* 6 (2016) 6124–6134.
- [32] A. Aronne, M. Turco, G. Bagnasco, G. Ramis, E. Santacesaria, M. Di Serio, E. Marenga, M. Bevilacqua, C. Cammarano, E. Fanelli, Gel derived niobium-silicon mixed oxides: characterization and catalytic activity for cyclooctene epoxidation, *Appl. Catal. A Gen.* 347 (2008) 179–185.
- [33] S.T. Oyama (Ed.), *Mechanisms in Homogeneous and Heterogeneous Epoxidation Catalysis*, Elsevier, Amsterdam, 2008.
- [34] N. Rösch, C. Di Valentin, I.V. Yudanov, in: F. Maseras, A. Lledós (Eds.), *Computational Modelling of Homogeneous Catalysis*, Kluwer Academic Publishers, Dordrecht, 2002, Ch. 12, pp. 289–324.
- [35] N. Antonova, J.J. Carbó, U. Kortz, O.A. Kholdeeva, J.M. Poblet, Mechanistic insights into alkene epoxidation with H₂O₂ by Ti- and other TM-containing polyoxometalates: role of the metal nature and coordination environment, *J. Am. Chem. Soc.* 132 (2010) 7488–7497.
- [36] L. Que Jr., W.B. Tolman, Biologically inspired oxidation catalysis, *Nature* 455 (2008) 333–340.
- [37] K.P. Bryliakov, E.P. Talsi, Active sites and mechanisms of bioinspired oxidation with H₂O₂, catalyzed by non-heme Fe and related Mn complexes, *Coord. Chem. Rev.* 276 (2014) 73–96.
- [38] M. Ziolk, P. Decyk, I. Sobczak, M. Trejda, J. Florek, H. Golinska, W. Klimas, A. Wojtaszek, Catalytic performance of niobium species in crystalline and amorphous solids-gas and liquid phase oxidation, *Appl. Catal. A Gen.* 391 (2011) 194–204.
- [39] M. Ziolk, I. Sobczak, P. Decyk, K. Sobanska, P. Pietrzyk, Z. Sojka, Search for reactive intermediates in catalytic oxidation with hydrogen peroxide over amorphous niobium(V) and tantalum(V) oxides, *Appl. Catal. B Environ.* 164 (2015) 288–296.
- [40] D.T. Bregante, P. Priyadarshini, D.W. Flaherty, Kinetic and spectroscopic evidence for reaction pathways and intermediates for olefin epoxidation on Nb in BEA, *J. Catal.* 348 (2017) 75–89.
- [41] I.D. Ivanchikova, M.K. Kovalev, M.S. Mel'gunov, A.N. Shmakov, O.A. Kholdeeva, User-friendly synthesis of highly selective and recyclable mesoporous titanium-silicate catalysts for the clean production of substituted p-benzoquinones, *Catal. Sci. Technol.* 4 (2014) 200–207.
- [42] T.R. Hughes, H.M. White, A study of the surface structure of decaionized Y zeolite by quantitative infrared spectroscopy, *J. Phys. Chem.* 71 (1967) 2192–2201.
- [43] C.A. Emeis, Determination of integrated molar extinction coefficients for infrared absorption bands of pyridine adsorbed on solid acid catalysts, *J. Catal.* 141 (1993) 347–354.
- [44] F. Thibault-Starzyk, B. Gil, S. Aiello, T. Chevreau, J.-P. Gilson, In situ thermogravimetry in an infrared spectrometer: an answer to quantitative spectroscopy of adsorbed species on heterogeneous catalysts, *Micropor. Mesopor. Mater.* 67 (2004) 107–112.
- [45] M. Tamura, K. Shimizu, A. Satsuma, Comprehensive IR study on acid/base properties of metal oxides, *Appl. Catal. A Gen.* 433–434 (2012) 135–145.
- [46] E.A. Paukshtis, E.N. Yurchenko, Study of the acid-base properties of heterogeneous catalysts by infrared spectroscopy, *Russ. Chem. Rev.* 52 (1983) 242–258.
- [47] E.A. Paukshtis, *Infrakrasnaya Spektroskopiya v Geterogennom Kislotno-Osnovnom Katalize (Infrared Spectroscopy in Heterogeneous Acid-Base Catalysis)*, Nauka, Novosibirsk, 1992 (in Russian).
- [48] V.N. Panchenko, M.M. Matrosova, J. Jeon, J.W. Jun, M.N. Timofeeva, S.H. Jung, Catalytic behavior of metal-organic frameworks in the Knoevenagel condensation reaction, *J. Catal.* 316 (2014) 251–259.
- [49] I.Y. Skobelev, O.V. Zalomaeva, O.A. Kholdeeva, J.M. Poblet, J.J. Carbó, Mechanism of thioether oxidation over di- and tetrameric Ti centres: kinetic and DFT studies based on model Ti-containing polyoxometalates, *Chem. Eur. J.* 21 (2015) 14496–14506.
- [50] G.B. Shul'pin, Metal-catalyzed hydrocarbon oxygenations in solutions: the dramatic role of additives: a review, *J. Mol. Catal. A Chem.* 189 (2002) 39–66.
- [51] H. Knözinger, Infrared spectroscopy for the characterization of surface acidity and basicity, in: G. Ertl, H. Knözinger, F. Schüth, J. Weitkamp (Eds.), *Handbook of Heterogeneous Catalysis*, second ed., Wiley-VCH, Weinheim, 2008, p. 1135.
- [52] M. Trejda, A. Tuel, J. Kujawa, B. Kilos, M. Ziolk, Niobium rich SBA-15 materials – preparation, characterisation and catalytic activity, *Micropor. Mesopor. Mater.* 110 (2008) 271–278.
- [53] F. Tielens, T. Shishido, S. Dzwigaj, What do the niobium framework sites look like in redox zeolites? A combined theoretical and experimental investigation, *J. Phys. Chem. C* 114 (2010) 3140–3147.
- [54] A. Ramanathan, R. Mageshwar, D.H. Barich, B. Subramanian, Niobium incorporated mesoporous silicate, Nb-KIT-6: synthesis and characterization, *Micropor. Mesopor. Mater.* 190 (2014) 240–247.
- [55] M. Ziolk, I. Sobczak, I. Nowak, P. Decyk, A. Lewandowska, J. Kujawa, Nb-containing mesoporous molecular sieves—a possible application in the catalytic processes, *Micropor. Mesopor. Mater.* 35 (36) (2000) 195–207.
- [56] M. Ziolk, I. Sobczak, A. Lewandowska, I. Nowak, P. Decyk, M. Renn, B. Jankowska, Oxidative properties of niobium-containing mesoporous silica catalysts, *Catal. Today* 70 (2001) 169–181.
- [57] J. Datka, A.M. Turek, J.M. Jehng, I.E. Wachs, Acidic properties of supported niobium oxide catalysts: an infrared spectroscopy investigation, *J. Catal.* 135 (1992) 186–199.
- [58] H. Zhu, A. Ramanathan, J.F. Wu, R.V. Chaudhari, B. Subramanian, Effects of tunable acidity and basicity of Nb-KIT-6 catalysts on ethanol conversion: experiments and kinetic modeling, *AlChE J.* 63 (2017) 2888–2899.
- [59] N.N. Trukhan, A.A. Panchenko, E. Roduner, M.S. Melgunov, O.A. Kholdeeva, J. Mrowiec-Bialoń, A.B. Jarzębski, FTIR spectroscopic study of titanium-containing mesoporous silicate materials, *Langmuir* 21 (2005) 10545–10554.
- [60] E.A. Paukshtis, N.S. Kotsarenko, L.G. Karakchiev, Investigation of proton-acceptor properties of oxide surfaces by IR spectroscopy of hydrogen-bonded complexes, *React. Kinet. Catal. Lett.* 12 (1979) 315–319.
- [61] R.A. Sheldon, M. Wallau, I.W.C.E. Arends, U. Schuchardt, Heterogeneous catalysts for liquid-phase oxidations: philosophers' stones or Trojan horses?, *Acc Chem. Res.* 31 (1998) 485–493.
- [62] P. Atkins, J. De Paula, *Elements of Physical Chemistry*, sixth ed., Oxford University Press, 2013.
- [63] W. Yan, A. Ramanathan, P.D. Patel, S.K. Maiti, B.B. Laird, W.H. Thompson, B. Subramanian, Mechanistic insights for enhancing activity and stability of Nb-incorporated silicates for selective ethylene epoxidation, *J. Catal.* 336 (2016) 75–84.
- [64] S.K. Maiti, A. Ramanathan, W.H. Thompson, B. Subramanian, Strategies to passivate Brønsted acidity in Nb-TUD-1 enhance hydrogen peroxide

- utilization and reduce metal leaching during ethylene epoxidation, *Ind. Eng. Chem. Res.* 56 (2017) 1999–2007.
- [65] P. Chagas, H.S. Oliveira, R. Mambriani, M. Le Hyaric, M.V. de Almeida, L.C.A. Oliveira, A novel hydrophobic niobium oxyhydroxide as catalyst: Selective cyclohexene oxidation to epoxide, *Appl. Catal. A Gen.* 454 (2013) 88–92.
- [66] H. Shima, M. Tanaka, H. Imai, T. Yokoi, T. Tatsumi, J.N. Kondo, IR observation of selective oxidation of cyclohexene with H₂O₂ over mesoporous Nb₂O₅, *J. Phys. Chem. C* 113 (2009) 21693–21699.
- [67] C.W. Yoon, K.F. Hirsekorn, M.L. Neidig, X. Yang, T.D. Tilley, Mechanism of the decomposition of aqueous hydrogen peroxide over heterogeneous TiSBA15 and TS-1 selective oxidation catalysts: insights from spectroscopic and density functional theory Studies, *ACS Catal.* 1 (2011) 1665–1678.
- [68] R.A. Sheldon, J.K. Kochi, *Metal-Catalyzed Oxidations of Organic Compounds*, Academic Press, New York, 1981.
- [69] M. Guidotti, E. Gavrilova, A. Galarneau, B. Coq, R. Psaro, N. Ravasio, Epoxidation of methyl oleate with hydrogen peroxide. The use of Ti-containing silica solids as efficient heterogeneous catalysts, *Green Chem.* 13 (2011) 1806–1811.
- [70] O.A. Kholdeeva, V.A. Grigoriev, G.M. Maksimov, M.A. Fedotov, A.V. Golovin, K.I. Zamaraev, Polyfunctional action of transition metal substituted heteropolytungstates in alkene epoxidation by molecular oxygen in the presence of aldehyde, *J. Mol. Catal. A Chem.* 114 (1996) 123–130.
- [71] L.J. Burcham, J. Datka, I.E. Wachs, In situ vibrational spectroscopy studies of supported niobium oxide catalysts, *J. Phys. Chem. B* 103 (1999) 6015–6024.
- [72] X.T. Gao, I.E. Wachs, M.S. Wong, J.Y. Ying, Structural and reactivity properties of Nb-MCM-41: comparison with that of highly dispersed Nb₂O₅/SiO₂ catalysts, *J. Catal.* 203 (2001) 18–24.
- [73] A. Wojtaszek, M. Ziolek, F. Tielens, Probing acid–base properties in group V aluminum containing zeolites, *J. Phys. Chem. C* 116 (2012) 2462–2468.
- [74] D.C. Tranca, A. Wojtaszek-Gurdak, M. Ziolek, F. Tielens, Supported and inserted monomeric niobium oxide species on/in silica: a molecular picture, *Phys. Chem. Chem. Phys.* 17 (2015) 22402–22411.
- [75] M.G. Clerici, Oxidation of saturated hydrocarbons with hydrogen peroxide, catalysed by titanium silicalite, *Appl. Catal.* 68 (1991) 249–261.
- [76] M.G. Clerici, P. Ingallina, Epoxidation of lower olefins with hydrogen peroxide and titanium silicalite, *J. Catal.* 140 (1993) 71–83.
- [77] S. Bordiga, A. Damin, F. Bonino, G. Ricchiardi, C. Lamberti, A. Zecchina, The structure of the peroxo species in the TS-1 catalyst as investigated by resonant Raman spectroscopy, *Angew. Chem. Int. Ed.* 41 (2002) 4734–4931.
- [78] W. Lin, H. Frei, Photochemical and FT-IR probing of the active site of hydrogen peroxide in Ti silicalite sieve, *J. Am. Chem. Soc.* 124 (2002) 9292–9298.
- [79] S. Bordiga, A. Damin, F. Bonino, C. Lamberti, Single site catalyst for partial oxidation reaction: TS-1 case study, *Top. Organomet. Chem.* 16 (2005) 37–68.
- [80] R.L. Brutchey, D.A. Ruddy, L.K. Andersen, T.D. Tilley, Influence of surface modification of Ti–SBA15 catalysts on the epoxidation mechanism for cyclohexene with aqueous hydrogen peroxide, *Langmuir* 21 (2005) 9576–9583.
- [81] E. Gianotti, C. Bisio, L. Marchese, M. Guidotti, N. Ravasio, R. Psaro, S. Coluccia, Ti (IV) catalytic centers grafted on different siliceous materials: spectroscopic and catalytic study, *J. Phys. Chem. C* 111 (2007) 5083–5089.
- [82] M.K. Harrup, G.-S. Kim, H. Zeng, R.P. Johnson, D. VanDerveer, C.L. Hill, Triniobium polytungstophosphates. Syntheses, structures, clarification of isomerism and reactivity in the presence of H₂O₂, *Inorg. Chem.* 37 (1998) 5550–5556.
- [83] D. Bayot, B. Tinant, B. Mathieu, J.-P. Declercq, M. Devillers, Spectroscopic and structural characterizations of novel water-soluble peroxo [polyaminocarboxylato bis(N-oxido)]niobate(V) complexes, *Eur. J. Inorg. Chem.* 737–743 (2003).
- [84] A. Maniatakou, C. Makedonas, C.A. Mitsopoulou, C. Raptopoulou, I. Rizopoulou, A. Terzis, A. Karaliota, Synthesis, structural and DFT studies of a peroxoniobate complex of the biological ligand 2-quinaldic acid, *Polyhedron* 27 (2008) 3398–3408.
- [85] N. Adler, C.F. Hiskey, Spectra of the peroxy complexes of niobium in sulfuric acid, *J. Am. Chem. Soc.* 79 (1957) 1827–1830.
- [86] N. Adler, C.F. Hiskey, Composition of the peroxy complexes of niobium(V) in sulfuric acid, *J. Am. Chem. Soc.* 79 (1957) 1831–1834.
- [87] Y. Narendar, G.L. Messing, Synthesis, decomposition and crystallization characteristics of peroxo–citrate–niobium: an aqueous niobium precursor, *Chem. Mater.* 9 (1997) 580–587.
- [88] Q. Geng, Q. Liu, P. Ma, J. Wang, J. Niu, Synthesis, crystal structure and photocatalytic properties of an unprecedented arsenic-disubstituted Lindqvist-type peroxopolyoxoniobate ion: {As₂Nb₄(O₂)₄O₁₄H_{1.5}}^{4.5-}, *Dalton Trans.* 43 (2014) 9843–9846.
- [89] S.R. Gogoi, J.J. Boruah, G. Sengupta, G. Saikia, K. Ahmed, K.K. Bania, N.S. Islam, Peroxonio niobium(V)-catalyzed selective oxidation of sulfides with hydrogen peroxide in water: a sustainable approach, *Catal. Sci. Technol.* 5 (2015) 595–610.
- [90] A. Zecchina, S. Bordiga, C. Lamberti, G. Ricchiardi, C. Lamberti, G. Ricchiardi, D. Scarano, G. Petrini, G. Leofanti, M. Mantegazza, Structural characterization of Ti centres in Ti-silicalite and reaction mechanisms in cyclohexanone ammoxidation, *Catal. Today* 32 (1996) 97–106.
- [91] D.A. Ruddy, T.D. Tilley, Kinetics and mechanism of olefin epoxidation with aqueous H₂O₂ and a highly selective surface-modified TaSBA15 heterogeneous catalyst, *J. Am. Chem. Soc.* 130 (2008) 11088–11096.
- [92] O.V. Zalomaeva, N.N. Trukhan, I.D. Ivanchikova, A.A. Panchenko, E. Roduner, E. P. Talsi, A.B. Sorokin, V.A. Rogov, O.A. Kholdeeva, EPR study on the mechanism of H₂O₂-based oxidation of alkylphenols over titanium single-site catalysts, *J. Mol. Catal. A Chem.* 277 (2007) 185–192.
- [93] G.B. Payne, P.H. Deming, P.H. Williams, Reactions of hydrogen peroxide. VII. Alkali-catalyzed epoxidation and oxidation using a nitrile as co-reactant, *J. Org. Chem.* 26 (1961) 659–663.
- [94] M. Guidotti, C. Pirovano, N. Ravasio, B. Lazzaro, J.M. Fraile, J.A. Mayoral, B. Coq, A. Galarneau, The use of H₂O₂ over titanium-grafted mesoporous silica catalysts: a step further towards sustainable epoxidation, *Green Chem.* 11 (2009) 1421–1427.
- [95] S. Ueno, K. Yamaguchi, K. Yoshida, K. Ebitani, K. Kaneda, Hydrotalcite catalysis: heterogeneous epoxidation of olefins using hydrogen peroxide in the presence of nitriles, *Chem. Commun.* 295–296 (1998).
- [96] M.A. Aramendía, V. Borau, C. Jiménez, J.M. Luque, J.M. Marinas, J.R. Ruiz, F.J. Urbano, Epoxidation of limonene over hydrotalcite-like compounds with hydrogen peroxide in the presence of nitriles, *Appl. Catal. A Gen.* 216 (2001) 257–265.
- [97] M.D. Romero, J.A. Calles, M.A. Ocaña, J.M. Gómez, Epoxidation of cyclohexene over basic mixed oxides derived from hydrotalcite materials: activating agent, solvent and catalyst reutilization, *Micropor. Mesopor. Mater.* 111 (2008) 243–253.
- [98] M.N. Timofeeva, A.E. Kapustin, V.N. Panchenko, E.O. Butenko, V.V. Krupskaya, A. Gil, M.A. Vicente, Synthetic and natural materials with the brucite-like layers as high active catalyst for synthesis of 1-methoxy-2-propanol from methanol and propylene oxide, *J. Mol. Catal. A Chem.* 423 (2016) 22–30.